Atmos. Chem. Phys. Discuss., 15, 16775–16859, 2015
www.atmos-chem-phys-discuss.net/15/16775/2015/
doi:10.5194/acpd-15-16775-2015

Atmospheric Chemistry and Physics Discussions

On measurements of aerosol–gas composition of the atmosphere during two expeditions in 2013 along Northern Sea Route

S. M. Sakerin[1], A. A. Bobrikov[2], O. A. Bukin[2], L. P. Golobokova[3], Vas. V. Pol'kin[1], Vik. V. Pol'kin[1], K. A. Shmirko[4,5], D. M. Kabanov[1], T. V. Khodzher[3], A. N. Pavlov[4], V. L. Potemkin[3], and V. F. Radionov[6]

[1]V. E. Zuev Institute of Atmospheric Optics, Siberian Branch, Russian Academy of Sciences, Tomsk, Russia
[2]Admiral G. I. Nevelsky State Marine University, Vladivostok, Russia
[3]Limnology Institute, Siberian Branch, Russian Academy of Sciences, Irkutsk, Russia
[4]Institute of Automatics and Control Processes, Far East Branch, Russian Academy of Sciences, Vladivostok, Russia
[5]Far East Federal University, Vladivostok, Russia
[6]Arctic and Antarctic Research Institute, St. Petersburg, Russia

Received: 29 December 2014 – Accepted: 18 May 2015 – Published: 19 June 2015

Correspondence to: S. M. Sakerin (sms@iao.ru)

Published by Copernicus Publications on behalf of the European Geosciences Union.

ACPD
15, 16775–16859, 2015

Abstract

We presented the results of expedition measurements of the set of physical-chemical characteristics of atmospheric aerosol in water basins of Arctic and Far East seas, performed onboard RV *Akademik Fedorov* (17 August–22 September 2013) and RV *Professor Khljustin* (24 July–7 September 2013). The specific features of spatial distribution and time variations of aerosol optical depth (AOD) of the atmosphere in the wavelength range of 0.34–2.14 µm and boundary layer height, aerosol and black carbon mass concentrations, and disperse and chemical composition of aerosol are discussed. Over the Arctic Ocean (on the route of RV *Akademik Fedorov*) there is a decrease in aerosol and black carbon concentrations in northeastern direction: higher values were observed in the region of Spitsbergen and near the Kola Peninsula; and minimum values were observed at northern margins of the Laptev Sea. Average AOD (0.5 µm) values in this remote region were 0.03; the aerosol and black carbon mass concentrations were 875 and 22 ng m^{-3}, respectively. The spatial distributions of most aerosol characteristics over Far East seas show their latitudinal decrease in the northern direction. On transit of RV *Professor Khljustin* from Japan to Chukchi Sea, the aerosol number concentration decreased, on the average, from 23.7 to 2.5 cm^{-3}, the black carbon mass concentration decreased from 150 to 50 ng m^{-3}, and AOD decreased from 0.19 to 0.03. We analyzed the variations in the boundary layer height, measured by ship-based lidar: the average value was 520 m, and the maximal value was 1200 m. In latitudinal distribution of the boundary layer height, there is a characteristic minimum at latitude of $\sim 55^{\circ}$ N. For water basins of eight seas, we present the chemical compositions of water-soluble aerosol fraction (ions, elements) and small gaseous impurities, as well as estimates of their vertical fluxes. It is shown that substances are mainly (75–89 %) supplied from the atmosphere to the sea surface together with small gaseous impurities. The deposited ions account for from 11 to 24.5 %, and trace elements account for 0.2–0.4 %. The average vertical fluxes of aerosol substance are a factor of 4–7 larger in the Japan Sea than in the water basins of Arctic seas.

ACPD
15, 16775–16859, 2015

1 Introduction

Studies of environment, including aerosol, in polar regions are urgent for two main reasons: (1) climate changes, which are most apparent just at high latitudes (Alekseev et al., 2011; Eisenman et al., 2007; IPCC, 2007); and (2) the beginning development of Arctic basin. One of the most dynamical environmental components is aerosol, which plays an important role in radiative transfer and mass exchange processes in the continent–atmosphere–ocean system. The radiative processes are usually separated into direct and indirect effects of aerosol (Haywood and Boucher, 2000; Kondratyev, 2002, 2006). The direct radiative effects are manifested in redistribution of scattered and absorbed solar radiation in the Earth's atmosphere. The indirect effects are associated with aerosol influence on the processes of cloud formation, cloud microphysical properties, rainfall, etc. (Twomey, 1977; Albrecht, 1989; Johnson et al., 2004).

Aerosol also influences substantially the processes of exchange of chemical compounds and elements between continent and ocean. Studies, performed by different authors, showed that transport of substances in aerosol composition via atmospheric channel is ranked second behind river discharge in significance (e.g., Shevchenko et al., 2000; Rahn, 1981). Transport of Saharan dust to Atlantic water basin (as far away as American coasts) by the trade wind, and the transport of Asian aerosol to Pacific and Indian Oceans by monsoons, are examples of the most powerful continental flows.

As to air transports from Eurasia to high latitudes, they are unstable and less intense; however, the aerosol sources in the neighboring regions, i.e., in polar and midlatitude zones, are very contrasting. On one hand, own aerosol in Arctic is practically absent because of snow-covered surface and low temperatures and insolation; on the other hand, the aerosol content is relatively high in boreal zone and, especially, in industrially developed regions of Europe. Under the influence of circulations, the Arctic atmosphere is enriched by aerosols of different types; smoke (forest fires), industrial, sulfate, organic, and other aerosols, including their absorbing components: black car-

ACPD
15, 16775–16859, 2015

bon (e.g., Vinogradova, 2014; Vinogradova and Veremeichik, 2013; Huang et al., 2010; Wang et al., 2011). The long-range meridional transports of aerosol substance occur predominately during winter and in submicron particle sizes range. A consequence of outflows is the change in radiative characteristics of the Arctic atmosphere (including clouds); while sedimentation of absorbing aerosol leads to a reduction in snow surface albedo, temperature rising, and ice and snow melt, i.e., just to those processes the role of which is least studied at present (IPCC, 2013).

No less attention was devoted recently to studying the atmospheric trace gas constituents (Duce, 1991; Jacob, 2000; Redington and Derwent, 2002), the content of which grew due to industrial activities and is considered by many experts as the main reason for global warming (IPCC, 2007, 2013). The interest in these studies in Arctic is associated with estimates of methane emissions in the regions of gas-and-oil fields, as well as with the effect of natural factors, i.e., with methane releases from gas-hydrates in shelf zone, during permafrost melt in subpolar region, and transports of dissolved methane by Siberian rivers (Sasakawa et al., 2010; Dmitrenko et al., 2011; Shakhova et al., 2010; Petrenko et al., 2010).

Even if ecological requirements are satisfied, the development of Arctic shelf and Northern Sea Route will elevate, to some or another degree, the aerosol–gas loading and will lead to additional effects which are still difficult to predict due to data shortage. Therefore, it is important to have more complete information on the present-day state of the Arctic atmosphere even at initial stage and to control its dynamics subsequently.

The aerosol observations are most long-term at the Arctic stations in Barrow (Alaska), Allert (Canada), Ny Alesund and Hornsund (Spitsbergen), and Sodankylä (Finland). The obtained results were reviewed, e.g., in works (Tomasi et al., 2007, 2012). The characteristics of the Arctic aerosol had been extensively studied by Russian scientists on a few high-latitude islands and at “North pole” drifting stations in 1970s–1990s (Radionov et al., 1994; Radionov and Marshunova, 1992; Tomasi et al., 2007). The results of the studies of polar aerosol in the next decade were summarized in reviewing monograph (Shevchenko, 2006).

ACPD
15, 16775–16859, 2015

The geography of aerosol studies in polar and subpolar regions of Russia had been substantially extended in the last period of time. In 2003–2007, a few cycles of expedition measurements of microphysical and chemical composition of aerosol were performed onboard research vessels in water basins of the White and Kara Seas (Polkin et al., 2007, 2011a; Golobokova et al., 2013). Regular observations of the aerosol optical depth (AOD) of the atmosphere in the regions of Tiksi (since 2010) and Yakutsk (since 2004) (Sakerin et al., 2005) had been initiated with the use of CE 318 Sun-Sky radiometer of AERONET network. Integrated studies of aerosol characteristics at the Russian polar station in Barentsburg (Spitsbergen) had been resumed (Sakerin et al., 2012, 2014).

In summer of 2013, the aerosol characteristics were measured in two Arctic cruises of research vessels (RV) *Akademik Fedorov* and *Professor Khljustin*. The physical-chemical characteristics of aerosol seem to be obtained for the first time within relatively short (about one-month) time interval along the entire Northern Sea Route from Arkhangelsk to Vladivostok. The main results of these studies are discussed in this work.

2 Characterization of expedition measurements

The route of RV *Akademik Fedorov* (Fig. 1) followed predominately in latitudinal direction: from Arkhangelsk to Kirkenes across the White and Barents Seas, and then across the Arctic Ocean to northeastern margins of the Laptev Sea and back. The route of RV *Professor Khljustin* followed in the meridional direction from Vladivostok to Bering Strait and then westward up to the port of Pevek (East Siberian Sea). The total periods of measurements were from 17 August to 22 September onboard RV *Akademik Fedorov* and from 24 July to 7 September onboard RV *Professor Khljustin*. The research program included the measurements of microphysical characteristics and chemical composition of aerosol in the near-ground layer, spectral AOD, and water va-

ACPD
15, 16775–16859, 2015

por content of the atmosphere. The height of the atmospheric boundary layer was additionally measured onboard RV *Professor Khljustin*.

The measurements of AOD and water vapor content of the atmosphere were performed using portable sun photometers SPM, operating in the wavelength range of 0.34–2.14 µm (Sakerin et al., 2013). The main technical characteristics of SPM are presented in Table 1. The measurements of direct solar radiation in the atmospheric "transparency windows" were used to calculate the spectral AOD and the parameters α, β of Ångström formula, which well describes the wavelength dependence of AOD in the wavelength region of ~ 0.3–1 µm:

$$\tau^{a}(\lambda) = \beta \cdot \lambda^{-\alpha} \quad (1)$$

The measurements in the IR wavelength range (1.2–2.14 µm) had made it possible to extract the coarsely dispersed AOD component τ^{c}, caused by quasi-neutral attenuation of radiation by large particles, as well as the selective finely dispersed AOD component $\tau^{f}(\lambda)$. For instance, in the region of 0.5 µm: $\tau^{f}(0.5) = \tau^{a}(0.5) - \tau^{c}$.

The total water vapor content of the atmosphere was determined on the basis of differential method according to data of measurements in water vapor absorption band (0.94 µm) and in the neighboring "transparency window" of 0.87 µm. The methods for determining AOD (including τ^{c}, τ^{f}) and water vapor content of the atmosphere, as well as the results of their analysis in different regions of ocean, were considered in more detail in works (Kabanov et al., 2009; Sakerin and Kabanov, 2002; Sakerin et al., 2008).

The microphysical characteristics of aerosol in the near-ground atmospheric layer were determined using two sets of instrumentation (Kozlov et al., 2010), comprising the photoelectric particle counters and aethalometers (see Table 1).

The mass concentration of absorbing substance (black carbon, BC) in the composition of aerosol particles M_{BC} (µg m^{-3}) was measured with the MDA-02 aethalometer at the wavelengths of 0.46, 0.53, 0.59, and 0.63 µm developed by IAO SB RAS (Kozlov et al., 2008, 2014). The concentration sensitivity of the aethalometer at 30 L of air pumped through the optical cell was about 10 ng m^{-3}. The aethalometer has been

ACPD
15, 16775–16859, 2015

calibrated under laboratory conditions through comparison of the data of synchronous optical and gravimetric measurements with a pyrolysis generator of soot particles. Additionally, intercalibration measurements of BC mass concentrations were performed with a MAAP-5012 aethalometer (Thermo Fisher Scientific Inc., Franklin, TN, USA).

The mass M_A (ng m^{-3}) and number N_A (cm^{-3}) concentrations of aerosol particles with diameters from 0.3 to 20 µm were determined with the help of photoelectric particle counters GRIMM 1.108 (Peters et al., 2006; Grimm and Eatough, 2009) and AZ-10 (Manual AZ-10, 2010), which were calibrated under factory conditions with the help of polystyrene latexes with known sizes. The intercalibration of photoelectric counters, performed before the expeditions, confirmed that data well compare within the uncertainties of the instruments.

The samples of the studied air were taken through silicon hoses with lengths up to 1 m for aethalometers and up to 0.5 m for particle counters. The heights of air sampling above the sea surface level were about 8 m onboard RV *Professor Khljustin* and 20 m onboard RV *Akademik Fedorov*. The aerosol parameters were measured around-the-clock, with the periodicity of the measurement cycles being one hour and with the duration being from 10 to 30 min, depending on the total particle concentration. The process of measurements is automated: it is performed in programmatically specified mode, with data being saved to files on computer. Processing was performed by sorting out separate measurements, distinctly burdened by the effect of local sources of aerosols of anthropogenic origin (exhausts from pipes of internal combustion engines, ventilation shafts, etc.). Sometimes, 20–30 % of the total data volume was sorted out with respect to separate parameters.

About 800 one-hour cycles of M_A, N_A, and M_{BC} measurements were performed onboard RV *Akademik Fedorov* for 30 days of measurements. After sorting out, 72 % of M_A, N_A values and 50 % of M_{BC} values left for analysis. About 900 measurement cycles were performed onboard RV *Professor Khljustin* for 46 days. A total of 77 % of M_A, N_A values and 67 % of M_{BC} values left for analysis after sorting out.

ACPD
15, 16775–16859, 2015

Samples of aerosol and gas admixtures for chemical analysis were collected on filter pack with the use of filter pack method, adopted in the international monitoring networks (EMEP, 1996). The total aerosol of coarsely and finely dispersed fractions was accumulated on PTFE filters (teflon, Japan) with pore diameters of 0.8 µm (filter no. 1). The gas admixtures (SO_2, HCl, NO_x, NH_3) were collected on polyamide filter ULTIPOR N with pore diameter of 0.45 µm (filter no. 2) and cellulose filter papers "Whatman" impregnated with an alkaline solution (filter no. 3) and an acid solution (filter no. 4).

In aqueous extract of filter no. 1, we determined the water-soluble fraction of aerosol substance, i.e., the ions of calcium (Ca^{2+}), magnesium (Mg^{2+}), sodium (Na^+), potassium (K^+), ammonium (NH_4^+), and nitrate (NO_3^-), chloride (Cl^-), and sulphate (SO_4^{2-}) ions. The analysis was performed by ion chromatography method on ion chromatography system ICS-3000 (Dionex, USA) (ICS-3000 Ion, 2008). The method of mass spectrometry with inductively coupled plasma on "Agilent 7500 ce" device (USA) was used to determine the content of water-soluble microelements Al, Ti, V, Cr, Fe, Co, Ni, Cu, Zn, As, Se, Mo, Cd, Sb, Pb, Ba, Be, B, Li, Mn, Sr, U. In aqueous extracts of filter no. 2 we measured the concentrations of ions SO_4^{2-}, Cl^-, NO_3^-, and NH_4^+ with a subsequent recalculation to give SO_2, HCl, HNO_3, and NH_3; and in aqueous extracts of filter no. 4 we measured the concentrations of ion NH_4^+ recalculated to give NH_3. The exposed filter no. 3 was extracted by 0.05 % hydrogen peroxide (H_2O_2) with a subsequent determination of concentration of ion SO_4^{2-} in the extract with recalculation to give SO_2 (EMEP, 1996). Before chemical analysis, all samples were filtered through acetate filter ("Vladisart", Russia) with pore diameter of 0.2 µm.

Onboard RV *Professor Khljustin*, we additionally collected aerosol samples on modified channel of impactor, which makes it possible to cut off particles larger than 1 µm in diameter and deposit finely dispersed fraction on filter (Polkin et al., 2011a). As a booster air flow, air pump NVM 1.2 with the pumping rate of 0.02 $m^3\,min^{-1}$ was used on the filter pack, and aspirator A-01 with the pumping rate of 0.005 $m^3\,min^{-1}$ was used on impactor. Aerosols were accumulated on filters for 8–10 h. The air analyzed was taken through silicon hose with diameter of 5 mm. The effect of the ship engine

ACPD
15, 16775–16859, 2015

exhaust plume was eliminated through a constant control of wind direction and synchronization of measurements with meteorological parameters obtained from meteorological station. In all, 38 samples of aerosols and gas admixtures were collected during expedition onboard RV *Professor Khljustin*, and 18 samples onboard RV *Akademik Fedorov*.

We note that that the reliability of chemical analysis results, obtained with these methods and instruments, was repeatedly confirmed through participation in data quality control (QA/QC) as part of international programs (http://qasac-americas.org; http://www.acap.asia/~interlab/os/; http://www.nilu.no; http://kvina.niva.no/intercomparison2). The data obtained largely deviate from true values by no more than 10–15 %, indicating the high quality of personnel and reliability of results.

In addition to aerosol characteristics, the height of the atmospheric boundary layer (BL) was measured in expedition cruise of *Professor Khljustin* with the help of one-frequency polarization lidar (Bukin et al., 2007; Shmirko et al., 2010). The receiver system of lidar comprised 150 mm telescope of Maksutov system, coupled with HAMMAMATSU R7400 photomultiplier tube (PMT) and high-speed two-channel analog-to-digital converter (ADC) of LA-n10-12USB-U trademark (http://www.rudshel.ru/board_with_USB.html). The Nd:YAG laser Brilliant-Ultra of Quantel firm (http://www.lambdaphoto.co.uk/pdfs/Ultra.pdf) with the generator of second harmonics was used as transmitter. The full overlap range was 80 m. The BL height was measured in the absence of dense low-level clouds, under calm-sea conditions three times a day: at the morning (08:00 UTC+11), dinner (13:00 UTC+11), and evening (22:00 UTC+11) hours. One-time measurement series lasted for about 8 min, during which we recorded 80 profiles at laser pulse repetition rate of 20 Hz. The backscattered signal with parallel and perpendicular polarizations was recorded by accumulating 100 shots. The measurements were performed along slant path with zenith angle of 42°. Each measurement series was accompanied by recording the profile, obtained with closed telescope, to account for correctly the background signal and various induced noises.

ACPD
15, 16775–16859, 2015

The optical experiments onboard *Professor Khljustin* were accompanied by measurements of meteorological parameters with the help of AMK-03 automated meteorological complex (http://meteosap.ru/). The meteorological complex makes it possible to measure the air temperature with the uncertainty of ±0.3 °C at temperature $T < |30|$ °C, and with the uncertainty of ±0.5 °C at temperature $T > |30|$ °C, with working temperatures ranging from −50 to +50 °C; the horizontal wind speed WS in the range from 0.1 to 40 m s^{-1} with uncertainty of ±(0.1 + 0.02·WS) m s^{-1}; the horizontal wind direction with uncertainty of ±2°; the vertical wind speed w in the range from −15 to 15 m s^{-1} with uncertainty of ±(0.1 + 0.02w) m s^{-1}; the relative humidity RH of air in the range from 15 to 100 % with uncertainty of ±2.5 % at $T > 0$, and with uncertainty of ±5 % at $T \leq 0$; and the atmospheric pressure in the range from 693 to 1067 hPa with uncertainty of ±1 hPa.

The data of back trajectory analysis were provided by Hybrid Single Particle Lagrangian Integrated Trajectory Model (https://ready.arl.noaa.gov/HYSPLIT.php). The boundary layer height was calculated from meteorological parameters, using reanalysis data of European Center for Medium-Range Weather Forecasts (ECMWF, http://data-portal.ecmwf.int/).

3 Atmospheric AOD and boundary layer height

3.1 Specific features of spatial distribution of AOD and water vapor content of the atmosphere

Sun photometer measurements of atmospheric AOD at Arctic latitudes are difficult to make due to low elevation (or absence) of Sun for a considerable part of the year, severe weather conditions, clouds, and fogs. Therefore, data of coastal observations for the same period of time in Barentsburg (Spitsbergen), Tiksi, and Vladivostok were involved in analysis of ship-based measurements to gain more complete understanding of AOD along the route of expeditions.

ACPD
15, 16775–16859, 2015

The AOD measurements were performed using SPM photometer in Barentsburg, SP-9 photometer in Vladivostok (Sakerin et al., 2013); and the AOD measurements in the region of Tiksi were performed using CE 318 Sun-Sky radiometer (AERONET), operating in the wavelength range of 0.34–1.02 µm (Holben et al., 1998). The coordinates of the main regions and periods of measurements are presented in Table 2. The total period of photometric observations was 21 August–14 September 2013.

The average characteristics of atmospheric depth, calculated for different maritime regions, are presented in Table 3 and in Fig. 2. Comparative analysis of data obtained led to the following conclusions. In Arctic zone, higher values of spectral AOD and water vapor content of the atmosphere were observed in the region of Barentsburg: for instance, the average values were $\tau^{a}_{0.5} = 0.053$ in the visible wavelength range. These atmospheric turbidities seem to be due to aerosol outflows from the direction of Europe and due to the effect of local sources located at Spitsbergen archipelago. Close average AOD values ($\tau^{a}_{0.5} = 0.046$) were reported in works (Herber et al., 2002; Tomasi et al., 2012) for another station on Spitsbergen, namely, Ny-Alesund according to observations in summer-fall periods of 1991–2010.

The AOD characteristics in other Arctic regions, extending from Kara Sea to Chukchi Sea, differ insignificantly and have small values, a factor of 1.7–2.5 smaller than in European sector of Arctic (Spitsbergen). For instance, the average AOD values in the regions 2–5 were in the range of 0.026–0.038 in the wavelength region of 0.5 µm. In the shortwave part of the spectrum, slightly larger AOD values were observed on the coast of the Laptev Sea (Polyarka), seemingly due to the effect of finely dispersed continental aerosol, like in Barentsburg. We also note that the characteristics of atmospheric depth in Asian sector of Arctic and in subpolar Bering Sea (region 6) are practically the same.

The average AOD values in the Arctic zone (even including Spitsbergen) are approximately a factor of 5 smaller than in background midlatitude regions: for instance, AOD (0.5 µm) is 0.15 and, in particular, $\tau^{c} = 0.04$ and $\tau^{f} = 0.11$ in Tomsk in August–September (Andreev et al., 2012). The small AOD values in the studied regions were because during summer 2013 in the boreal part of Eurasia there were no severe for-

ACPD
15, 16775–16859, 2015

est fires, which affect appreciably the Arctic atmosphere (Stohl et al., 2006; Eck et al., 2009). These events in Eurasian part of Russia were last observed in 2010 and 2012 (Chubarova et al., 2012; Sakerin et al., 2014).

Results of AOD measurements onboard RV *Professor Khljustin* in Far East seas exhibited much stronger variations (Fig. 2b). In the spatial distribution, there is well apparent latitudinal dependence, with AOD and water vapor content increasing southward. All characteristics in the Bering Sea were the same as in Arctic, they were a factor of 1.5–2 larger near the southern coasts of Kamchatka, and the difference reached a factor of 4–6 in the region of Vladivostok.

Comparison of finely and coarsely dispersed components of AOD showed that their minimal values $\tau^{f} \approx 0.02$ and $\tau^{c} = 0.01$–0.015 are characteristic for Siberian Arctic and the subarctic Bering Sea. The τ^{c} value increases by about a factor of 2, and the τ^{f} increases by about a factor of 1.5–2 in the regions of Spitsbergen and southern coasts of Kamchatka; and their largest values are recorded in the region of Vladivostok. It is noteworthy that the strongest (a factor of 7) differences from Arctic zone are manifested in the value of finely dispersed component of AOD.

3.2 Variations in the atmospheric boundary layer height

Recent studies by different authors (Kay et al., 2011; Deser et al., 2010; Boé et al., 2009) showed that the processes, flowing in the lower atmosphere, are key to understanding and modeling the climate changes in Arctic. The climate models in northern regions are often much worse, because parameterizations of atmospheric boundary layer are largely based on observations at more southern latitudes. Studies of the boundary layer height in the Arctic atmosphere will make it possible to improve our understanding and to estimate the scale of the processes of momentum, energy, and water vapor exchange between underlying surface and the free troposphere.

ACPD
15, 16775–16859, 2015

3.2.1 Experimental data and method of boundary layer height determination

Atmospheric aerosol was used as a tracer of the boundary layer (BL). The BL height was determined by gradient (threshold) method according to measurements of the profiles of total depolarization of laser radiation:

$$\delta(h) = \frac{P_{\perp}(h)}{P_{\parallel}(h)} = \frac{\beta^{\pi}_{\perp}(h)}{\beta^{\pi}_{\parallel}(h)} \quad (2)$$

Here, $P_{\perp}(h)$ and $P_{\parallel}(h)$ are the cross- and parallel polarized components of backscattered signal, $\beta^{\pi}_{\perp}(h)$ and $\beta^{\pi}_{\parallel}(h)$ are the total (aerosol + molecular) backscattering coefficients of cross- and parallel polarized radiation respectively, and $\delta(h)$ is the coefficient of total depolarization of laser radiation.

The boundary layer height was assumed to be the height within the first 3000 m, for which the first derivative $\mathrm{d}\delta(h)/\mathrm{d}h$ had the global minimum. This method was successfully applied in our early works (Bukin et al., 2013; Pavlov et al., 2013; Shmirko et al., 2012). It is based on two statements: (1) concentration of aerosol particles sharply jumps at BL boundary; and (2) the depolarization degree of the aerosol atmosphere is larger than the depolarization degree of the purely molecular atmosphere.

Ship-based measurements of the marine BL height, carried out during the cruise, were compared against measurements with Cloud-Aerosol Lidar with Orthogonal Polarization (CALIOP) satellite lidar. The general characterization of the satellite measurement system, as well as the description of the products obtained, is presented in (http://www.nasa.gov/calipso; Powell et al., 2013). In this case, the BL height was identified using a modification of the method (Balin et al.; 2003), based on representation of BL as ground-adjacent air layer, the properties of which, due to intense turbulent mixing, are determined mainly by thermal and dynamical effects of the underlying surface.

The BL height is determined by calculating the matrix of interlevel correlation (Eq. 3) of time series of attenuated ratio (Total_Attenuated_Backscatter_532 L1B CALIPSO DATA) of scattering at the wavelength of 532 nm for different heights in a specified time

ACPD
15, 16775–16859, 2015

window:

$$\eta_{i,j} = \frac{\sum_{k=1}^{M}\left[\left(P'_{i,k} - \overline{P'_i}\right)\left(P'_{j,k} - \overline{P'_j}\right)\right]}{\sqrt{\sum_{k=1}^{M}\left(P'_{i,k} - \overline{P'_l}\right)^2 \cdot \sum_{k=1}^{M}\left(P'_{i,k} - \overline{P'_l}\right)^2}} \quad (3)$$

$$\overline{P'_{i(j)}} = \frac{1}{M}\sum_{k=1}^{M} P'_{i(j),k}, \quad (4)$$

where $P'_{i,k} = P'(z_i, t_k)$, $P'_{j,k} = P'(z_j, t_k)$, $\forall i < j[1 \ldots N]$, $k \in [1 \ldots M]$ is attenuated ratio of backscattering at the wavelength of 532 nm (Total_Attenuated_Backscatter_532). The matrix of interlevel correlation was calculated by considering only a fragment of signal, corresponding to the height interval of 100–4000 m ($N = 130$).

The higher the position of scattering layer, the weaker is its interrelation with underlying layers, which immediately affects the correlation coefficient. Therefore, with the availability of vertical profile of the coefficient of interlevel correlation, and after determining a certain threshold value of this coefficient, the vertical extents of BL can be found. The main feature of the method is its low sensitivity to random signal fluctuations; it works even when gradient methods fail. Despite these advantages, there is nonetheless the uncertainty regarding the choice of the critical value of the correlation coefficient. In the given case, the threshold correlation coefficient of 0.55 was determined by comparing the BL heights, measured by ship-based lidar, with the vertical profile of the coefficient of interlevel correlation. The algorithm for data processing consisted of the following stages:

1. Selection of data from spatiotemporal window ($M = 120$ points, 40 km) for regions, located over sea surface.

2. Cloud filtering (the data of measurements were removed from the sample if the profiles of attenuated backscattering contained quite intense peaks in this height interval).

ACPD
15, 16775–16859, 2015

3. Calculation of BL height (including calculation of the matrix of interlevel correlation, the average profile of interlevel correlation, and height satisfying the choice criterion).

4. Shift of the window by 1 profile (~ 333 m in the plane of the Earth).

5. Return to point 1.

The method described in works (Hennemuth and Lammert, 2006; Vogelezang and Holtslag, 1996; Menut et al., 1999; Troen and Mahrt, 1986) was used to retrieve the boundary layer height according to reanalysis data.

3.2.2 Spatiotemporal variations in the boundary layer height

Figure 3 illustrates the temporal and latitudinal variations in the BL height in the period of expedition of RV *Professor Khljustin*. The BL height (H_{BL}) varied in the wide range from 200 to 1200 m. The average height H_{BL} over the entire cruise was 520±195 m, and the most probable value was 612 m. The obtained quantitative characteristics correspond to literature data, suggesting that H_{BL} is on the average 420 m (Wang and Wang, 2004), ~ 800 m (Bradley and Keimig, 1993), and 934±300 m (Nilsson, 1996). The maximum value H_{BL} = 1200 m was observed on roadstead of port of Pevek throughout 21 August 2013.

As to the latitudinal distribution of H_{BL} (Fig. 3b), it exhibits the periodic regularity. Initially the BL height decreases with latitude up to 55° N; and then the trend becomes opposite. The BL heights were high in the region of Bering Strait, and then H_{BL} had somewhat decreased. Similar variations in the BL height were found in the Southern Hemisphere in the frameworks of Global Backscatter Experiment (GLOBE) (Menzies and Tratt, 1997). The BL subsidence rate is 25 m deg^{-1} on the first (43.1–55° N) and second (55–65° N) segments, and it becomes equal to 50 m deg^{-1} on the third segment (65–70° N).

ACPD
15, 16775–16859, 2015

The H_{BL} value behaves analogously in CALIPSO satellite data, with the only difference being that the dispersion of the data is not that much. For the water basin considered here (regions of northeastern part of Pacific Ocean and eastern Arctic), the boundary layer height, retrieved according to satellite data, and its latitudinal dependence are in good correspondence with ship-based measurements: the correlation coefficient is 0.5 at 0.95 significance level, and the critical value of the correlation coefficient for this sample is 0.24. The CALIPSO data also display the characteristic minimum of H_{BL} in the region of 55° N, with its subsequent growth in the northern direction.

The latitudinal decrease of the BL height is confirmed in the works (Zilitinkevich and Esau, 2009); however, the further H_{BL} growth (at latitudes poleward of 55° N) does not fit into the classical concept of the latitudinal BL variations and seems to be due to the specific character of the region (terrain topology, wind and temperature regimes, etc.). Despite the coincidence of H_{BL}, obtained by two methods, the probability remains for its overestimation at northern latitudes by virtue of specific features of the methods used. The method for determining H_{BL} from satellite data through the critical value of the coefficient of interlevel correlation is implicitly related to H_{BL}, determined according to ship-based lidar measurements.

The problem was resolved by calculating additionally the BL heights according to reanalysis data (the profiles of temperature and wind speed) (Hennemuth and Lammert, 2006; Vogelezang and Holstang, 1996; Menut et al., 1999; Troen and Mahrt, 1986). Since this method is based on model-derived meteorological parameters, it is less subject to the effect of local aerosol sources, land, and low clouds. The main sources of data for reanalysis are the stations of upper-air measurements. These stations are sparse in the study region and at all absent over sea. Therefore, the results of the BL height calculations should be interpreted as averages for this period. From Fig. 3b it can be evident (see the black line with triangles) that the latitudinal distribution of the BL height somewhat differs from analogous data of satellite and ship-based measurements: the H_{BL} variations are not strongly pronounced, and their amplitude does not exceed 200 m.

ACPD
15, 16775–16859, 2015

Reanalysis data suggest that the BL height decreases from 500 to 400 m as latitude changes from 40 to 53° N, and further northward it remains at practically the same level. The maximum differences in H_{BL}, obtained by different methods, are observed in southern (~ 45° N) and northern (~ 67° N) parts of the region analyzed. In the southern part, the decreased H_{BL} values, calculated according to reanalysis data, can be ascribed to the specific character of ECMWF data. At Arctic latitudes, higher H_{BL} values, calculated according to data of CALIPSO and ship-based lidar, seem to be due to increased influence of land (Chukchi Peninsula).

To understand the reasons for these spatial BL variations, we analyzed the back trajectories of motion of air masses (https://ready.arl.noaa.gov/HYSPLIT.php), calculated for every hour of expedition measurements. Analysis was made for three segments of the route: (1) the region of small H_{BL} values at the 55° N latitude, (2) the region of high H_{BL} on the territory of Bering Strait; and (3) the region of extremely high H_{BL} values in the area of Pevek. The back trajectory analysis gave the following results (Fig. 4).

The boundary layer height was relatively small (~ 380–400 m), if the wind blew from the direction of open ocean (Fig. 4a), or if the air masses passed over water surface during most of the time on preceding day (Fig. 4b). Otherwise, if the trajectories of air motion passed over the land (Fig. 4c and d), a higher level of H_{BL} values (~ 800 m) was observed. The largest BL height (~ 1200 m) was recorded on roadstead of port of Pevek, when air propagated over land from the direction of the city (Fig. 4d). The local temperature field is, on the average, 3–4° higher in city; therefore, higher H_{BL} values should be expected on lee side.

4 Aerosol and black carbon contents in the near-ground atmospheric layer

4.1 Specific features of spatial aerosol variations in Arctic seas

The routes of expedition cruises of RVs *Akademik Fedorov* and *Professor Khljustin* encompass quite large (no less than five thousand km) territory in Arctic zone, pre-

ACPD
15, 16775–16859, 2015

determining the need to identify separate regions (and datasets) for interpreting the aerosol microphysical characteristics.

Preliminary analysis of measurements onboard RV *Akademik Fedorov* showed that the latitudinal and meridional dependences in N_A, M_A, and M_{BC} concentrations were not explicitly present, but separate parameters somewhat decreased in northeastern direction. That is, the effect of continental aerosol sources weakened with distance from Scandinavian coasts. Based on the findings above, in the Arctic zone we singled out the following four regions (their geographic positions are indicated in Fig. 1):

- K – water basin of the Barents Sea near Kola Peninsula coasts;
- B – the Barents Sea – Western sector of Arctic;
- A – the Arctic ocean – northern margins of the Kara and Laptev Seas;
- F – the East Siberian and Chukchi Seas – Far East sector of Arctic.

The statistical characteristics of N_A, M_A, and M_{BC} for these regions, calculated according to diurnally average values, are presented in Table 4. As expected, the highest average concentrations of aerosol and black carbon and the widest variability ranges were observed near Kola Peninsula (region K). The average values of all characteristics decreased with distance from Scandinavia, but differently with respect to separate parameters. The largest changes occurred in absorber content. The average M_{BC} value in the region B decreased by a factor of 2.5, and it decreased by another factor of 2.5 in the region A (on the whole, M_{BC} decreased by more than a factor of 6 relative to the region K).

The number and mass concentrations of aerosol decreased by 15 and 28 % respectively only in passage from the Kola Peninsula to high-latitude part of the Barents Sea. The difference in N_A and M_A concentrations between Arctic regions B and A was found to be insignificant, much less than the standard deviation.

Also, the table presents the statistical characteristics of aerosol and black carbon concentrations, measured onboard RV *Professor Khljustin* in Far East sector of Arctic

ACPD
15, 16775–16859, 2015

(region F). We note the following specific features of aerosol parameters in this region. The average concentration M_{BC} has quite a low value, occupying an intermediate position between data in the regions B and A. The number concentration N_A turned out to be the lowest, and the mass concentration M_A turned out to be the highest among other Arctic regions.

This opposite difference between N_A and M_A in Far East sector of Arctic was due to the specific features of hydrometeorological conditions, which led to the corresponding features of the aerosol disperse composition. The period of changes in the Chukchi and East Siberian Seas was characterized by relatively frequent fogs and stronger sea surface roughness. As is well known (Reist, 1993; Rasool, 1973), both these factors favor the increase in the content of coarsely dispersed aerosol, which makes major specific contribution to aerosol mass concentration.

From comparison of the average particle distributions over volumes dV/dr (Fig. 5) it can be seen that measurements in the region F indeed were characterized by elevated content of larger particles in the size range $r > 0.7\,\mu m$ and by decreased content of small particles ($r < 0.3\,\mu m$). Relatively large aerosol concentrations in the entire particle size range were recorded on the segment of the route near the Kola Peninsula. Evidently, this disperse composition was explained by the effect of aerosol outflows from continent, as well as by the generation of maritime aerosol under the conditions of developed sea roughness.

The smallest-valued and practically identical distributions dV/dr were observed in high-latitude Arctic regions B and A, primarily because of their remoteness from continental aerosol sources, low temperatures, and weak generation of maritime aerosol on largely ice- and snow-covered territories.

Comparison of distributions dV/dr, obtained during Arctic expeditions in 2013, against the data of preceding studies in the White and Kara Seas, and in Tiksi (June 2010) and Barensburg (July 2011) (Polkin et al., 2011a; Sakerin et al., 2012) has led to the following conclusions (see Fig. 5). The average dV/dr in high-latitude regions decrease in northeastern direction (in accordance with influence degree of the

ACPD
15, 16775–16859, 2015

sources of continental aerosol), and the range of their difference reaches two orders of magnitude. The maximal particle concentrations in the entire size range are characteristic for subpolar and, virtually, internal White Sea. Intermediate values of particle concentration were observed in Kara Sea and on Spitsbergen archipelago (Barentsburg), and the lowest level was observed over Arctic Ocean and in Tiksi. Low concentration of submicron particles in the region of Tiksi (June 2010) can be explained by relatively low air temperature under the conditions when a major part of coastal zone of sea and tundra were still covered by ice and snow (Sakerin et al., 2012).

On the whole, the average values of the concentrations N_A, M_A, and M_{BC}, obtained in the regions K, B, A, and F, agree with studies by other authors in the Russian sector of Arctic. For instance, the average number concentrations of 4–8 cm^{-3}, i.e., close to our data, were obtained in ground-based measurements on Franz Josef Land (Zigler Isl., spring 1994; Smirnov et al., 1998). However, at the same time, the aerosol mass concentration turned out to be much higher: (25–50) $\times 10^3$ $ng\,m^{-3}$. The authors explained the elevated mass concentrations by the presence of soil-derived particles in the region of measurements.

Ship-based measurements of black carbon mass concentration during fall of 1998 in the Barents Sea (Kopeikin et al., 2010) showed that the average values of M_{BC} varied from 160 $ng\,m^{-3}$ during northerly and northeasterly winds to 980 $ng\,m^{-3}$ when wind blows from the Western Siberia. Based on aircraft measurements in April 1992 over the East Siberian Sea (Hansen et al., 1997), the average values of M_{BC} in the near-ground layer (height of $\sim$ 100 m) were about 150 $ng\,m^{-3}$. Lower values of black carbon concentration, equaling $\sim$ 8 $ng\,m^{-3}$ for the summer period, were presented in work (Sharma et al., 2004) on the basis of data of multiyear (1989–2002) measurements at Alert station, Canada.

ACPD
15, 16775–16859, 2015

4.2 Latitudinal dependence of aerosol and black carbon distributions in Far East seas

The route of RV *Professor Khljustin* followed predominately in meridional direction from Vladivostok to port of Pevek, through the Japan, Okhotsk, Bering, Chukchi, and East Siberian Seas (Fig. 1). The time behavior of aerosol and black carbon concentrations for the entire period of expedition is presented in Fig. 6. We should turn attention to strong variations in the parameters N_A, M_A, and M_{BC}, which were caused by diurnal and synoptic changes in the hydrometeorological conditions. In all study regions, the variations in each parameter within 1–3 days exceed one order of magnitude, and the total variability ranges were: from 0.003 to 90.2 cm^{-3} for N_A; from 1 to 13 630 $ng\,m^{-3}$ for M_A; and from 2 to 400 $ng\,m^{-3}$ for M_{BC}. Even when the data are averaged over separate sea water basins (shown by circles), the average aerosol characteristics markedly differ between forward and backward routes.

In particular, the average values of aerosol number and mass concentrations over the Japan Sea turned out to be about a factor of 2 larger at the beginning of cruise than on backward route. This difference was because of the stronger sea roughness (Beaufort numbers of 3–4) and the corresponding generation of large particles of maritime aerosol. In addition, outflows of submicron aerosol from the direction of continent had a stronger effect at the beginning of cruise. The specific features of the average disperse composition of aerosol on forward and backward routes for two seas are illustrated in Fig. 7.

From the figure it can be seen that, in the range of large particles, the volume distributions dV/dr over the Okhotsk Sea are approximately an order of magnitude larger on the backward route than on the forward route, primarily because sea was strongly roughed after typhoon passage. Because of the substantial predominance of coarsely dispersed particles, the average mass concentration M_A in this case turned out to be the highest (13 630 $ng\,m^{-3}$) over the entire period of measurements.

ACPD
15, 16775–16859, 2015

Thus, the short periods of measurements in separate water basins on forward and backward routes (from 3 to 9 days), given the high variability of the studied parameters, turn out to be insufficient to obtain a reliable information on the average characteristics of aerosol in any region. Nonetheless, in the variations of the aerosol parameters we discern a decrease during first half of the cruise (which followed northward) and an increase in the aerosol and black carbon concentrations on return back.

The aerosol parameters were diurnally averaged to mitigate the effect of short-period variations. Analysis of regression dependences of the diurnally average values of N_A, M_A, and M_{BC} on the geographic latitude ϕ (Fig. 8) confirms that these values tend to decrease in the northern direction. The equations of the linear regression of separate parameters are presented in the upper part of the figure, and the correlation coefficients for regression lines are indicated in parentheses. We note that the latitudinal dependences for all aerosol parameters are statistically significant. In this case, the level of statistically significant correlation is 0.3 with 0.95 confidence probability.

To obtain the quantitative data on the spatial distribution of aerosol characteristics, the average values of N_A, M_A, and M_{BC} were additionally calculated within four latitude zones 42 – 46.5 – 52 – 67 – 71° N, which approximately correspond to separate seas: the Japan, Okhotsk, Bering, Chukchi, and East Siberian Seas. The obtained average values of aerosol parameters are presented in Table 5 and shown in Fig. 8 by thick lines. From the figure it can be seen that the latitudinal decrease is more firmly manifested for aerosol number concentration and black carbon mass concentration: N_A decreased from 23.7 cm^{-3} over the Japan Sea to 2.5 cm^{-3} over the Chukchi Sea (by about a factor of 9), and M_{BC} decreased from 149 to 51 $ng\,m^{-3}$ (by about a factor of 3).

In the variations of aerosol mass concentration M_A, there was also first a decrease, followed by a minor growth in passing to higher latitudes. This behavior is explained by the redistribution of contributions of fine and coarse aerosols to M_A, primarily due to the specific hydrometeorological conditions during cruise. The large concentration of submicron aerosol over the Japan Sea (for a moderate content of large particles) ensured the relatively high average level of M_A. In passing to the Okhotsk Sea, and

ACPD
15, 16775–16859, 2015

then to the Chukchi and Bering Seas, the content of small particles had substantially decreased, so that the value of M_A had been determined only by variations in coarsely dispersed aerosol, generated from the sea surface. Its concentration at high latitudes remained at quite a high level due to wind-driven roughness; therefore, no M_A decrease occurred.

We know nothing about analogous studies by other authors in these regions. Data of our measurements onboard the sailing vessel "Nadezhda" in water basin of the Okhotsk Sea in August 2010 (Polkin et al., 2011b) can only be presented for comparison purposes. The average values of aerosol parameters, obtained in this expedition ($N_A = 40.6\,cm^{-3}$; $M_A = 8000\,ng\,m^{-3}$; $M_{BC} = 520\,ng\,m^{-3}$), are several-fold larger than the data of measurements onboard RV *Professor Khljustin* in 2013. The differences in hydrometeorological conditions and routes between the two cruises (regions of measurements) explain these discrepancies. A considerable part of data in August 2010 was obtained near the islands of Kuril chain and Sakhalin, with a larger influence of continental sources. In this case, the maximum concentrations reached the following values: $N_A = 350\,cm^{-3}$; $M_A = 141\,000\,ng\,m^{-3}$; and $M_{BC} = 19\,000\,ng\,m^{-3}$. In addition, the conditions of measurements were characterized by more frequent fogs and high relative humidity of air. That is, the data of the two expeditions do not contradict each other, but just indicate the strong dependence of aerosol characteristics on the effects of outflows of continental aerosol and meteorological conditions.

4.3 Effect of meteorological conditions on aerosol number concentration in cruise of RV *Professor Khljustin*

As is well known, the concentration of aerosols in the atmosphere is caused not only by the intensity of emissions from different sources, lifetime, and particle transformation, but also by meteorological conditions: wind, humidity, rainfall, characteristics of air flows (trajectories, transport height), etc. These factors differently influence the content of aerosol particles with diverse sizes. Therefore, below we will consider not only the total

ACPD
15, 16775–16859, 2015

number concentration N_A, but also the concentrations of submicron N_f ($0.3\,\mu m \le d \le 1.0\,\mu m$) and coarsely dispersed N_c ($1.0\,\mu m < d \le 10\,\mu m$) fractions: $N_A = N_f + N_c$.

Figure 9 shows the time behavior of characteristics, measured in the period of expedition: number concentrations of submicron and coarsely dispersed aerosol; volume particle size distributions; relative humidity; and wind speed. Also shown in the figure are characteristics, calculated according to 72 h back trajectories of air mass motion (using data at http://ready.arl.noaa.gov/HYSPLIT.php): the total along-trajectory rainfall amount and the fraction of trajectories passing over land.

The relative air humidity was close to 100 % in the period of expedition; nonetheless, dips, caused by arrival of dryer continental air masses at the region of measurements, can be periodically seen on the plot. The wind speed varied in the wide range, from perfect calm to $20\,m\,s^{-1}$. The particle number concentration is most dynamical variable among aerosol microphysical parameters (Figs. 6a, 9a and b). The range of N_A variations over the entire period of expedition was more than 4 orders of magnitude. The mass concentrations M_A and M_{BC} varied less strongly (Fig. 6b and c), approximately in the ranges of 3 and 2 orders of magnitude respectively.

The specific features of variations in the concentrations of separate fractions N_f and N_c in different regions will be analyzed below; and first we will estimate the effect of the meteorological parameters on the total concentration N_A over the entire period of measurements. For this, we considered a regression model with the use of available data on wind speed WS, water temperature, air temperature T, rainfall amount RF, and fraction of trajectories passing over land. To construct the regression equation, we used an iteration algorithm which sought the approximation coefficients and discrepancy at each step by least squares method. Data (bursts) were excluded from the initial sample if the discrepancy exceeded three standard deviations (SD). The calculations continued until no bursts remained. As a result, we obtained a model which depended on just three parameters:

$$N_A = 0.645 + 0.209 \cdot \mathrm{WS} - 0.104 \cdot T + 0.018\mathrm{RF} \quad (5)$$

ACPD
15, 16775–16859, 2015

Comparison of results of model calculations with N_A measurements (Fig. 10) showed a good agreement in the cases when: the effect of continental sources was weak; the wind speed was relatively low ($0.5 < WS < 10\,m\,s^{-1}$), which ensured a linear relationship with aerosol concentration; air temperature was in the range of $-2.5 < T < 16\,^{\circ}C$ and rainfall was in the range $0 < RF < 44\,mm\,h^{-1}$. The correlation coefficient of regression model is 0.71 under these conditions (the number of points is 330). That is, Eq. (5) can be used to estimate the particle number concentration, based on three meteorological parameters: WS, $\cdot T$, and RF. The model gives incorrect results when the data of trajectory analysis and ion composition of aerosol samples indicate the effect of continent, as well as in the proximity to large-scale atmospheric vortices (cyclones).

According to the total set of the average meteorological conditions and the intensity of sources of continental aerosol, the middle and Arctic latitudes have differences, which could not help being reflected in specific features of behavior of the number concentrations of submicron (Fig. 9a) and coarsely dispersed (Fig. 9b) aerosol fractions in these regions. The N_f concentration substantially changed at the beginning and end of the expedition (midlatitudes); while in the middle part (high latitudes), the variability range and the average level of N_f decreased by approximately a factor of three. Except in the first day of measurements, the concentration of coarsely dispersed fraction remained at low level until 10 August, and increased afterward.

These same features are also traced according to the character of change in the aerosol disperse composition (Fig. 9c). The highest dV/dr values, with predominance of submicron aerosol, were observed at the beginning and end of cruise, when vessel was at midlatitudes, in proximity to and surrounded by the land. That is, the aerosol content was formed under the influence of outflows of finely dispersed aerosol from relatively well developed regions. The remaining period, especially when the vessel was in the Arctic zone, was characterized by low content of aerosol, with a larger contribution of coarsely dispersed fraction.

Thus, the relative contents of large and small particles are redistributed in the aerosol in passing from middle to high latitudes. The observed increase in the relative role of

ACPD
15, 16775–16859, 2015

large particles in subarctic and Arctic regions was noted as early as in (O'Dowd and Smith, 1993) and is explained by predominance pf maritime air masses.

The division of data into two groups (zones) according to the relative contents of two aerosol fractions is clearly confirmed by scatter diagram of N_f and N_c values (Fig. 11) in the zones of midlatitude (red) and Arctic (blue) latitudes. The slope coefficient of regression line for the first group of data, obtained in the period from 24 July to 10 August and 3–7 September, is $\gamma = N_c/N_f = 10^{-2}$. A less slope of regression line is caused by dominating contribution of submicron aerosol at midlatitudes. Low content of coarsely dispersed maritime aerosol (see Fig. 9b) also explained why the values of the parameter γ were low at the beginning of the expedition (until 10 August). This aerosol was weakly generated because of small wind speed (Fig. 9d).

These measurements in Arctic and subarctic regions (on 10–31 August) were characterized by low values of the number concentration and a relative importance of coarsely dispersed fraction, indicating the predominance of maritime aerosol (Bigg et al., 1995; Nilsson et al., 2001). The slope coefficient of regression line is $\gamma = 4.5 \times 10^{-2}$ in this case.

The lowest concentrations of the two fractions were observed from 5 to 10 August (Bering Strait and Chukchi Sea): the average value of N_f was 0.65 cm^{-3}; and coarsely dispersed particles, despite wind strengthening, were practically absent. This was favored by the washing-out action of rainfall (see Fig. 8e) and supply of clean Arctic air from the direction of Chukchi Peninsula (Fig. 5c). Here, it is important to note that the effect of outflows of continental air is diverse in different regions. At midlatitudes, the outflows considerably enrich the marine atmosphere by finely dispersed aerosol (most characteristically, the outflows of Asian aerosol to the Japan Sea). In poorly developed continental Arctic, the aerosol sources are substantially weakened or absent. Therefore, the outflows of air masses from the direction of land (Fig. 5c and d) do not lead to increase of aerosol content in sea water basins.

ACPD
15, 16775–16859, 2015

5 Chemical composition of the atmosphere on the route of RV *Akademik Fedorov*

5.1 Ion composition of aerosol

The samples of aerosol substance and gaseous impurities in the Arctic atmosphere were taken along forward and backward routes of RV *Akademik Fedorov* (see Fig. 1). Four regions of the Arctic Ocean were singled out for analysis of aerosol chemical composition. The first region was the water basin of the Barents Sea (region B), in which one aerosol sample was obtained on the way forth and another on the way back. We considered in more detail the data in high-latitude part of the route (region A); here, we singled out three sub-regions: A_1, i.e., the Arctic Ocean (northward of Severnaya Zemlya and Franz Josef Land archipelagos, 81–84° N, 68–111° E); A_2, i.e., the northwestern part of the Laptev Sea (77–80° N, 107–126° E); and A_3, i.e., the northeastern margins of the Laptev Sea (78–81° N, 127–155° E).

The averaged characteristics of ion composition of aerosols for these regions are presented in Table 6. Analysis was performed excluding samples, obtained under unfavorable weather conditions, when marine component (Na^+, Cl^-) in the chemical composition of aerosol was an order of magnitude higher than other ions.

From these results it can be seen that the concentrations of most ions were somewhat higher in northwestern part of the Laptev Sea (sub-region A_2) among other high-latitude regions. However, the existing differences in concentrations are not large and much smaller than the standard deviations. More salient differences in ion composition of aerosol are characteristic for water basin of Barents Sea (region B), showing approximately two times larger values of both the total content and concentrations of separate (except K^+) ions. In addition to low concentrations of ions over Barents Sea, we also note a considerable difference in ion composition of aerosol on the routes forth (21–23 August 2013) and back (20–21 September 2013). For instance, the concentrations of ions of alkali-earth components and ions Cl^- were two or more times larger at the beginning of the cruise than on the way back. The air masses arrived at the

ACPD
15, 16775–16859, 2015

region of the Barents Sea (both near the Earth's surface and at the 850–700 hPa isobaric surface) mainly from direction of the Scandinavian Peninsula and northern coast of Russia.

Despite the relatively large variations in ion concentrations, the marine component, i.e., sodium and chloride ions, was found to predominate throughout the route. Their percentage was maximal and equaled 22–33 % of the total sum of ions for sodium and about 43 % for chlorides. For other ions, in order of decreasing concentrations, there had been the following sequence: $NH_4^+ > K^+$, $Mg^{2+} > Ca^{2+}$, and $SO_4^{2-} > NO_3^-$. In earlier publications (Polkin et al., 2011a), based on analysis of integrated dispersion parameter of distribution, filling factors, and chemical composition of soluble fraction of aerosols, for the water basins of the White and Kara Seas it was shown that ions Cl^-, Na^+, and Ca^{2+} are contained mainly in coarsely dispersed particles, while the ions SO_4^{2-} and NH_4^+ are mainly present in finely dispersed aerosol.

In polar regions, seawater is not the only source of salt aerosol. To determine its origins, we used the well-known formulas to calculate the percentages of sea-salt (ss-) and non-sea-salt (nss-) sulphates and calcium (EMEP, 1996):

$$\left[\text{nss-}SO_4^{2-}\right] = \left[SO_4^{2-}\right] - 0.06028 \cdot [Na^+]$$

$$\left[\text{ss-}SO_4^{2-}\right] = \left[SO_4^{2-}\right] - \left[\text{nss-}SO_4^{2-}\right] \quad (6)$$

$$[\text{nss-}Ca^{2+}] = [Ca^{2+}] - 0.02161 \cdot [Na^+]$$

$$[\text{ss-}Ca^{2+}] = [Ca^{2+}] - [\text{nss-}Ca^{2+}], \quad (7)$$

where $\left[SO_4^{2-}\right]$ is the sulphate concentration, $[Na^+]$ is the sodium concentration in aerosol; 0.06028 is the relationship of concentrations SO_4^{2-}/Na^+ for ions of seawater, 0.02161 is the relationship of concentrations Ca^{2+}/Na^+ for ions of seawater; the initial content of components is represented in molar concentration (mol L^{-1}).

The obtained results showed that seawater was the main source of sulphates in almost 40 % of the cases. The largest number of samples with high ss-SO_4^{2-} was col-

ACPD
15, 16775–16859, 2015

lected in sub-region A_2. The average content of ss-SO_4^{2-} in this region was about 80 % of the total sulphate concentration in aerosol. The minimal concentrations of ss-SO_4^{2-} in aerosol were recorded in the northernmost region A_1. The relationship of concentrations ss-SO_4^{2-}/nss-SO_4^{2-} (3 : 1) was most stable in the eastern part of the route (region A_3).

On the whole, the chemical composition of aerosol is similar to that of seawater with respect to the relative content of anions (Turekian, 1968). That is, we can conclude that sea-salt particles make a major contribution to the chemical composition of aerosols in the Arctic sector under study. The sources of nss-SO_4^{2-} in maritime aerosol are the processes of washing out of SO_2 by atmospheric precipitation and the processes of oxidation of SO_2 and dimethyl sulfide (DMS), which is produced by sea plankton algae. The formation of nss-SO_4^{2-} from DMS is identified according to the presence of methanesulfonic acid (MSA). The presence of MSA was recorded in the first half of expedition when ship passed along the Severnaya Zemlya archipelago (24.0 ng m^{-3}), in coastal part of the Laptev Sea (2.87 ng m^{-3}), and in the region A_3 (0.01–3.69 ng m^{-3}).

The maximal average percentage of ss-Ca^{2+} in aerosol composition over the water basin of the Laptev Sea was 48 % of the total calcium concentration. In other regions, the percentage of maritime calcium was even lower and equaled ~ 32 %. It is well known that series of concentrations of elements in seawater and maritime aerosol coincide. According to the Dittmar law, the quantitative relationships between principal components of the main salt composition are always constant in seawater samples. We quantitatively estimated the differences in relationships of the Ca^{2+}, K^+, Mg^{2+}, Cl^-, and SO_4^{2-} concentrations with respect to sodium ion in aerosol (aer) and seawater (sw):

$$K_i = \left[\left(C_i/\mathrm{Na}^+\right)_{\mathrm{aer}}\right] / \left[\left(C_i/\mathrm{Na}^+\right)_{\mathrm{sw}}\right], \quad (8)$$

where (C_i/Na^+) is the concentration of the ith element with respect to Na^+, and K is the enrichment coefficient (Tsunogai et al., 1972). The enrichment coefficient makes it possible to estimate the contributions of different sources to the chemical composition

ACPD
15, 16775–16859, 2015

of aerosol. A considerable excess of the enrichment coefficient indicates that certain elements in the study region are continental in origin.

The obtained data showed that the ratios $(K^+/Na^+)_{aer}$ and $(Ca^{2+}/Na^+)_{aer}$ are much higher in aerosol than in seawater. The maximal enrichment of aerosol, particularly by potassium (by up to a factor of 18), was observed on 23–24 August 2013 at the northern margins of Kara Sea (in the region of Severnaya Zemlya islands). The air masses on these days arrived from north of Krasnoyarsk Krai and Severnaya Zemlya. On the average, $(K^+/Na^+)_{aer}$ exceeded $(K^+/Na^+)_{sw}$ by a factor of 2.5, and $(Ca^{2+}/Na^+)_{aer}$ exceeded $(Ca^{2+}/Na^+)_{sw}$ by a factor of 3.1. The enrichment of aerosol particles by chlorides and sulphates is less pronounced. The excess of chlorides was, on the average, a factor of 1.2, and the excess of sulphates was a factor of 1.3.

5.2 Elemental composition of aerosol

First measurements of elemental composition in solid-phase aerosol, performed in 1985–1988 on the Wrangel and Severnaya Zemlya islands, made it possible to obtain information on aerosol composition and sources in the Russian sector of Arctic. These data were used to determine: the mineral and chemical composition of solid-phase aerosol, the aerosol particle size distribution, the transport pathways of eolian material, and the degree of pollution of the Arctic atmosphere by anthropogenic pollutants; also, these data were used to identify the groups of elements associated with terrigenous (Fe, Al, Mn), marine (Na, Cl), and anthropogenic (Co, Sb, Zn, Pb) sources (Shevchenko, 2006; Vinogradova and Ponomareva, 2007).

In oceanic water, practically all elements are in dissolved form and play an important role in formation of the chemical composition of maritime aerosol. Based on measurements in cruise of *Akademik Fedorov*, we analyzed the elemental composition in water-soluble fraction of aerosol. The percentage of microelements in this fraction varied from 0.3 to 9.9 % of the total number of soluble inorganic components. The obtained results (see Table 7) were characterized by a great variety and a wide variability range of concentrations, reaching four-five orders of magnitude. Despite this, we can note that the

ACPD
15, 16775–16859, 2015

concentrations of most elements in the atmosphere of the Barents Sea are markedly smaller than in high-latitude regions of the Arctic Ocean (A_1–A_3). With respect to certain elements (Al, Ba, Cr, V, Br), no statistically significant differences between separate regions were manifested.

With respect to content of water-soluble elements in the aerosol composition, we can single out three groups: (1) with concentrations from several tens to several tenths of ng m^{-3}, (2) from several tenths to several hundredths of ng m^{-3}, and (3) from several thousandths to analytical zero. Metals of predominately terrigenous origin, i.e., Fe, Zn, Al, Ba, as well as Cu and Sr, refer to the first group. The elements in the first group totaled 93.4 % of all analyzed microelements. The second group included Ni, Cd, Cr, Se, Pb, V, Mo (5.6 % of the total composition), which are mostly the markers of anthropogenic pollution. The third group consists of Ti, Co, Sb, Li, As (0.6 % of the total composition). Elements in this group originate from both natural and anthropogenic sources.

In analogy to the main ions in aerosol, the enrichment coefficients of concentrations of elements were also calculated. High enrichment intensity was revealed for five elements: Fe, Zn, Cu, Cd, and Cr. Excess of the ratios of concentrations of elements in aerosol was observed along the entire route of the vessel, but the highest enrichment coefficients were recorded in the northernmost part in the period from 11 to 18 September. Partial enrichment of aerosol particles by the elements Al, Fe, Ni, Se, Ti, and Sb was revealed in separate samples. Among these elements, Fe, Al, and Ti are most widespread in the Earth's crust. Their average enrichment coefficients in aerosol were found to be 29.9, 5.0, and 4.8, respectively. The contents of such elements as Cu, Cd, Zn, Sb, Se, Ni, and Cr in aerosol composition are ascribed to both natural and anthropogenic sources (Vinogradova and Ponomareva, 2007). The enrichment coefficients of these elements varied in the following ranges: K = 2.0–34.4 for Cu, K = 8.8–794 for Cd, K = 4.8–72.8 for Zn, K = 1.1–9.1 for Sb, K = 1.1–4.4 for Se, K = 1.1–1.6 for Ni, and K = 1.2–264 for Cr.

ACPD
15, 16775–16859, 2015

Comparison of Na, Ca, Co, Ni, Se, As, Sr, Sb, and Ba concentrations in water-soluble fraction of aerosol with analogous elements in solid-phase aerosol (Goryunova and Shevchenko, 2008) indicates that dissolved components in aerosol composition have different contributions. For instance, this value was, on the average, 15 % for sodium, 13 % for calcium, and about 4 % for barium. The dissolved percentages of other elements vary between wider limits. The maximal percentage of 50 % is revealed for selenium, 15 % for nickel, and about 5 % for antimony. Cobalt accounted for ~ 2 %, arsenic accounted for a little more than 1 %, and strontium accounted for 1 %.

5.3 Small gaseous impurities

As is well known, small gaseous impurities have a significant effect on the chemical composition of the atmosphere. On the route of the expedition, the smallest content of gaseous impurities was observed in the atmosphere of the Barents Sea (Table 8). This result is consistent with the geographic distribution of concentrations of ions and most elements in aerosol composition (see Sects. 5.1 and 5.2). At the same time, we cannot rule out the possibility that the manifested significant difference in concentrations of ions, elements, and gaseous impurities in the atmosphere of the Barents Sea (as compared to more northern regions) could be not due to natural features, but rather due to small number of aerosol samples (2 filters).

In high-latitude regions, a higher content of gaseous impurities in the atmosphere was recorded in the northern and eastern parts of the route (regions A_1 and A_3). The maximal concentrations in these regions are characteristic for sulfur dioxide SO_2, among separate gases. Its main sources over ocean are evaporation of seawater, dimethyl sulfide generation by algae, and gas-phase conversions in the atmosphere. In the atmospheric composition, there are also nitrogen-containing gases, which participate, like SO_2, in acid sedimentation. Nitric acid (HNO_3), formed in the atmosphere, may long remain at gas-phase state because of its low condensation. In contrast to SO_2, the highest HNO_3 concentrations were observed in the region A_2. In addition to SO_2 and HNO_3, in the atmosphere of studied regions there is the hydrochloric acid

ACPD
15, 16775–16859, 2015

(HCl), which is formed via displacement by stronger acids (MSA, HNO_3, H_2SO_4) from NaCl, which enters into the composition of maritime aerosol. Ammonia (NH_3) is mainly supplied to the atmosphere as a result of biological decomposition of marine organic products (Behera, 2013).

Joint analysis of concentrations of the sum of ions in aerosol and small gaseous impurities in the atmosphere showed the presence of their interrelation (Fig. 12). The cross-correlation coefficient of these characteristics along the route of the expedition was 0.68.

5.4 Fluxes of chemical substances to sea surface

The obtained results were used to estimate the vertical fluxes of water-soluble substances to the sea surface. In the calculations, we used the values, known from literature data: the dry deposition velocity for the Arctic atmosphere in the summer period, equaling $3.4 \times 10^{-4}\,m\,s^{-1}$; dry deposition velocity geometric mean, equaling $1.9 \times 10^{-3}\,m\,s^{-1}$ for the open sea (Nilsson and Rannik, 2001); and deposition velocity of large (larger than 1 µm) particles, equaling $2 \times 10^{-2}\,m\,s^{-1}$ for coastal regions (Duce et al., 1991). In view of the fact that the fluxes, calculated for the sub-regions A_1, A_2, and A_3, turned out to be close, Table 9 presents only data for the region A as a whole.

Fluxes of substances, arriving from the atmosphere together with different ions (under heading Ions in Table 9) were determined for the sum of Cl, Na, K, Mg, Ca, N, and S. Nitrogen was recalculated in the sum of nitrates and ammonium ions, and sulfur was recalculated from sulphates. Fluxes of trace elements (TE) were calculated for the sum of Al, Ti, V, Cr, Fe, Co, Ni, Cu, Zn, As, Se, Mo, Cd, Sb, Pb, Ba, Be, Li, Mn, and Sr concentrations.

For substances, arriving together with gaseous impurities (GI), we took the sum of concentrations of elements Cl, N, and S, calculated from gaseous compounds HCl, (HNO_3+NH_3), and SO_2, respectively. The calculations show that substances are mostly supplied to the surface of Arctic seas together with gaseous impurities. On the average, according to the data of entire expedition, deposited ions accounted for about

ACPD
15, 16775–16859, 2015

24.5 %, trace elements accounted for 0.4 %, and small gaseous impurities accounted for 75 % of the total amount of water-soluble substances (Ions + TE + GI), arriving from the atmosphere.

For comparison purposes, Table 9 presents the fluxes of water-soluble substances from the atmosphere, calculated according to results of earlier studies in the water basins of the White and Kara Seas (Polkin et al., 2007, 2011a). Species fluxes in the Arctic cruise of RV *Akademik Fedorov* turned out to be approximately an order of magnitude lower than in more southern regions (65–77° N) of the White and Kara Seas, close to continent.

Separately, we considered the arrival of sulfur and nitrogen at the sea surface (the upper part of Table 10). As compared to the fluxes of aerosol substance, the arrival of nitrogen together with gaseous impurities is almost an order of magnitude higher, and arrival of sulfur is, on the average, a factor of 70 higher.

6 Chemical composition of the atmosphere on the route of RV *Professor Khljustin*

6.1 Ion composition of aerosol

The chemical composition of aerosol in cruise of RV *Professor Khljustin* was determined according to samples, collected on the filters PTFE for five Far East seas: the Japan, Okhotsk, Bering, Chukchi, and East Siberian Seas. The last two seas, though adjoining the Far East of Russia, refer to Arctic seas. We will use this name in the given paper just for brevity of the general name. The average concentrations of ions in aerosol composition over Far East seas are presented in Table 11 separately for the first and second halves of the cruise. From these data it can be seen that ion concentrations vary in quite a wide range. The average ion concentrations differ not only among separate seas, but also in the same regions on the forward and backward routes of the vessel. The ions Na^+, Mg^{2+}, K^+, Cl^-, and SO_4^{2-} exhibit the strongest vari-

ACPD
15, 16775–16859, 2015

ations. Nonetheless, for the first half of the cruise, the total sum of ions and contents of individual ions distinctly show a tendency of their latitudinal distribution (Fig. 13). As the ship moved from low to high latitudes, the total concentration of ions in the near-water aerosol decreased by approximately 30 %. A little weaker gradient (a decrease by ~ 13 %) was observed during transit from the Okhotsk to Bering Sea.

Data, collected on backward route of the vessel, exhibited stronger spatiotemporal variations in ion content, and the regularity of their latitudinal growth was not distinctly manifested. This was primarily because, on backward route, in the aerosol composition there was a much (a factor of 2–9) larger contribution from sea-derived ions, i.e., Na^+, Mg^{2+}, and Cl^-, the generation of which was caused by stronger sea surface roughness, rather than by the geographic position of the region. The strongest variations in the Na^+, Mg^{2+}, and Cl^- contents in aerosol composition were observed over the Okhotsk Sea. As was already noted in Sect. 4.2, due to large content of coarsely dispersed particles in this region, the aerosol mass concentration turned out to be the highest over the entire period of expedition.

To reveal the nature of the aerosol chemical composition on different sections of the route, Eqs. (6) and (7) were used to calculate the percentages of sea salt (ss-) and non-sea salt (nss-) ions SO_4^{2-} and Ca^{2+} for two aerosol fractions. When ship moved in the forward direction, the percentage of ss-SO_4^{2-} was maximal in finely dispersed fraction and increased to 100 % in water basins of the Bering, Chukchi, and East Siberian Seas. In samples with total aerosol (in two fractions), the percentage of ss-SO_4^{2-} was the largest on backward route of the ship. As was already noted above, coarsely dispersed particles predominated in aerosol composition. Hence, sea surface exerted the major influence on formation of the chemical composition of coarsely dispersed aerosol, especially in water basins of the Okhotsk and Japan Seas.

In remote maritime regions, one of the sources of nss-SO_4^{2-} is DMS, which is oxidized to give, in addition to other substances, methanesulfonic acid. The concentration of MSA in aerosol composition varied from 0.1×10^{-3} to 5.9×10^{-3} ng m^{-3}. The variability range of nss-SO_4^{2-} concentrations was 0.03–2.17 µg m^{-3}. The performed corre-

ACPD
15, 16775–16859, 2015

lation analysis revealed no interrelation between nss-SO_4^{2-} and MSA concentrations. Evidently, the nss-SO_4^{2-} ions were mostly continental in origin. The elevated percentage of nss-Ca^{2+} ions also indicates this. Continental sources had the largest effect on aerosol composition in the first half of cruise in the water basins of the Japan, Okhotsk, and East Siberian Seas, where the percentage of nss-Ca^{2+} reached 80–99 %. On backward route, the elevated percentage of nss-Ca^{2+} in aerosol composition was contained only over the Bering Sea.

The parallel use of impactor and filter pack, where the total aerosol was sampled (in contrast to expedition of RV *Akademik Fedorov*), has made it possible to calculate the enrichment coefficients from Eq. (8) separately for coarsely and finely dispersed aerosols. In the total aerosol, the maximal enrichment (K = 13–34) was revealed for ions K^+ over water basins of the Japan and Okhotsk Seas. Another component with high enrichment coefficient is calcium: the excess of $(Ca^{2+}/Na^+)_{aer}$ over $(Ca^{2+}/Na^+)_{sw}$ was a factor of 2–15. The maximal enrichment of sulphates in aerosol was revealed over the Bering Sea: the excess of $(SO_4^{2-}/Na^+)_{aer}$ over $(SO_4^{2-}/Na^+)_{sw}$ reached a factor of 67. This excess was, on the average, about a factor of 5 over the Sea of Japan, and a factor of 2–3 over other seas.

In finely dispersed aerosol fraction, the maximal enrichment was revealed for ions Ca^{2+}, except in the Bering Sea, where the enrichment prevailed for ions K^+. In this fraction a marked enrichment of ions SO_4^{2-} and Cl^- was also noted.

Because of the considerable dependence of aerosol characteristics on hydrometeorological conditions, given the limited time and the number of samples taken, we could not determine the average chemical composition, characteristic for separate seas. Therefore, we additionally averaged the ion concentrations over three largest sea water basins, where no less than one ten of aerosol samples was collected; these regions were: (1) remote regions of Arctic (region A, n = 14), which are less subject to the effect of continental aerosol outflows, while their own sources are weak, (2) polar and subpolar seas (the Chukchi and Bering Seas, n = 15), which, although located near Asian coasts, are nonetheless characterized by low-intensity aerosol sources, (3)

ACPD
15, 16775–16859, 2015

Far East seas at midlatitudes (the Japan and Okhotsk Seas, $n = 10$), most subject to the effect of continental aerosol outflows.

From these results (see Fig. 14) it follows that the average concentrations of most ions and their sum increase in the above-mentioned sequence of three regions. For instance, the summed concentration of ions, as compared to the Arctic Ocean, increases by 73 % over the Bering and Chukchi Seas, and by a factor of 2.5 over the Japan and Okhotsk Seas. Exceptions are the ions NH_4^+ and NO_3^-, the average concentration of which is most low over the Bering and Chukchi Seas (smaller than in remote regions of the Arctic Ocean). Another salient feature is characteristic for ions SO_4^{2-}, the concentration of which is nearly the same in southern and northern Far East seas.

The data, considered above, although not, either, being totally free of specific weather conditions during expeditions, nonetheless better reflect the real features of the average spatial distribution of ion concentrations over ocean.

6.2 Elemental aerosol composition

The statistical data on the concentrations of water-soluble microelements in the atmospheric aerosol over Far East seas are presented in Table 12. The variability range of the total microelement composition was 8.8–107.1 ng m^{-3}, with the general decreasing tendency with the growing latitude.

The percentage of water-soluble microelements over different sea water basins varied from 0.1 to 25 % of the total number of inorganic components. The largest percentage of microelements was contained in aerosol, sampled over Okhotsk and Chukchi Seas. With respect to the microelement concentrations, we can single out three groups: (1) Zn, Cu, Al, Fe, Ba, Mn, Sr, V, Ni, (2) Pb, Se, Cr, Cd, Sb, Li; and (3) As, Ti, Mo, Co, Be. Despite certain differences, the concentration distribution of elements over Far East seas is close to data, obtained in Arctic cruise of *Akademik Fedorov* (see Table 7).

Most elements exhibit a tendency of latitudinal decrease in concentrations from the Japan Sea to the Arctic Ocean; while Cd shows an opposite change (Fig. 15). The latitudinal distribution is broken up for the following elements: the minimal Fe, Se, Mo, Ti,

ACPD
15, 16775–16859, 2015

and Sb concentrations are observed in the subpolar Bering Sea; and Al concentrations peak in the Okhotsk Sea.

The microelement enrichment coefficients, calculated from Eq. (8), indicate the largest enrichment intensity for seven elements: Zn, Cu, Al, Fe, Mn, Cr, and Cd. With respect to intensity of pollution of aerosol by these elements the studied seas can be lined up in the following order: the Okhotsk, Chukchi, Japan, Bering, and East Siberian Seas. An important role in formation of air pollution level is played by the processes of trans-boundary transport of suspended particles and pollutants from adjoining territories. The Okhotsk and Bering Seas serve as a kind of water filter on the way of transit of airflows from Russia and Southeastern Asia toward the Pacific Ocean (Rudis, 2010). The Chukchi Sea, like a number of Arctic seas of Russia, is situated on the way of transit of contaminants from industrial regions of Russia, Europe, and America (Hov et al., 2007; Vinogradova, 2014). The Japan Sea is subject to anthropogenic impacts not only from regional sources, but also due to trans-boundary pollutant transport from China, Korea, and Japan (Luangjame, 2013; Toyama et al., 2013).

Comparative analysis of enrichment coefficients of microelements in separate seas has led to the following conclusions. The maximal ratios $K = (C_i/\mathrm{Na})_{\mathrm{aer}}/(C_i/\mathrm{Na})_{\mathrm{sw}}$, reaching tree-four orders of magnitude, are found for Zn and Cr. With respect to zinc, most severe atmospheric pollutions were observed over water basins of the Okhotsk (K = 36–1204) and Chukchi Seas (K = 23–1127). The Zn enrichment coefficients over other Far East seas varied within two orders of magnitude (K = 10–97). Pollution by chrome compounds was found to be maximal in the atmosphere of the Bering Sea (K = 10–1143). The Cr enrichment coefficients over other seas were as follows: K = 73–181 for the Japan Sea, K = 90–224 for the Okhotsk Sea, K = 21–106 for the Chukchi Sea, and K = 77 for the East Siberian Sea.

Large (as large as two-three orders of magnitude) enrichment for Cu was found over water basins of all Far East seas (K = 13–351), for Cd over the Okhotsk (K = 15–305) and Chuckchi Seas (K = 10–171), and for Al over the Okhotsk Sea (K = 42–328). We note that Cu and Cd are primarily markers of anthropogenic emission, while Al signifies

ACPD
15, 16775–16859, 2015

to a larger degree the terrigenous supply of particles to the atmosphere. The maximal enrichment of aerosol by manganese was revealed in aerosol over the Okhotsk (K = 194–217) and Chukchi (K = 10–223) Seas. An elevated intensity of aerosol enrichment by iron was observed over the Japan (K = 13–34), Okhotsk (K = 9–40), Chukchi (K = 10–34) Seas.

6.3 Small gaseous impurities

We had already indicated above the marked differences in the atmospheric conditions and aerosol composition between the first and second halves of the cruise of RV *Professor Khljustin*. Therefore, the concentrations of the small gaseous impurities were considered separately on the forward and backward routes of ship (Table 13). We can note the following features of the spatiotemporal variations in gaseous impurities.

At the beginning of the cruise, the average concentrations of HCl, SO_2, and HNO_3 substantially decreased in passage from relatively warm seas (the Japan and Okhotsk Seas) to Arctic seas (the Chukchi and East Siberian Seas). The average concentration of HCl decreased from ~ 25 to 2.7–6.2 $\mu g\,m^{-3}$, the average concentration of SO_2 decreased from 0.7–0.8 to ~ 0.1 $\mu g\,m^{-3}$, and the average concentration of HNO_3 decreased from ~ 0.7 $\mu g\,m^{-3}$ to analytical zero. No latitudinal variations in the concentration was found on backward route in passing from northern to southern seas, seemingly due to specific weather conditions. However, the weather conditions had no effect on NH_3 concentration, which was characterized by nearly the same low level of 0.03–0.05 $\mu g\,m^{-3}$ on the most of the route, in both forward and backward directions. Higher NH_3 concentrations, found to be 0.21 $\mu g\,m^{-3}$, were recorded only in Arctic zone, especially over the Chukchi Sea.

Joint analysis of variations in the SO_2 and MSA concentrations showed the presence of close interrelation with the correlation coefficient of 0.77 (Fig. 16). This may indicate that DMS is oxidized to give SO_2. Moreover, there was a weak negative correlation between the concentrations of NH_3 and sum of gases HCl, SO_2, and HNO_3.

ACPD
15, 16775–16859, 2015

From comparison with data of Arctic cruise *Akademik Fedorov* (see Table 8) it follows that the concentration of gaseous HCl is several-fold higher, and the concentrations of SO_2 and NH_3 are several-fold lower, over Far East seas.

6.4 Fluxes of chemical substances to water surface

In analogy to the data from expedition of RV *Akademik Fedorov* (see Sect. 5.4) we calculated the vertical fluxes of deposition of chemical substances to water surface of Far East seas (see lower part of Table 9). The obtained results showed that, like over Arctic seas, the substances are mainly supplied together with gaseous impurities (GI). Their relative contribution is 77–89 % of the total sum (Ions + TE + GI) of deposited water-soluble substances. The deposited ions in the aerosol composition account for from 11 to 23 %, and trace elements (TE) account for 0.2–0.4 %. The largest substance fluxes (Ions + TE + GI) were observed over water basin of the Japan Sea. About a factor of 4 less substance is deposited to the surface of the East Siberian Sea.

Comparison with data for remote regions of the Arctic Ocean (A_1–A_3) indicates that more impurities are deposited in coastal water basins of the Chukchi and East Siberian Seas. Despite the absence of well-developed industry on the Chukchi Peninsula, the proximity of continent has an effect on the formation of the chemical composition of the atmosphere and on the value of fluxes to adjoining seas.

Fluxes of sulfur and nitrogen compounds are especially important in the processes of mass exchange between the atmosphere and sea surface. On one hand, sulfur and nitrogen are the necessary components of organic world. The major suppliers of these elements under the Arctic conditions are the atmospheric fallouts (Shevchenko, 2006). On the other hand, the excessive concentrations of sulfur and nitrogen may have a negative environmental effect. Regeneration of sulfur and nitrogen compounds via photochemical processes in the atmosphere leads to formation of toxic impurities.

The calculations showed (see lower part of Table 10) that the vertical fluxes of nitrogen together with gaseous impurities are much higher than those together with aerosol substance: by a factor of 10 over the Japan and Bering Seas, by almost a factor of 50

ACPD
15, 16775–16859, 2015

over the water basin of the Okhotsk Sea, by more than a factor of 70 over the Chukchi Sea, and by a factor of 160 over the East Siberian Sea. In contrast to remote regions of the Arctic Ocean, the deposition fluxes of sulfur together with aerosol substance to the surface of Far East seas are larger than those together with gaseous impurities: by about a factor of 8 for the Japan Sea, and by about the factors of 6, 14, and 1.5 for the Okhotsk, Bering, and Chukchi Seas respectively.

7 Conclusions

In summer 2013, we carried out the integrated studies of the atmospheric aerosol in two cruises of RV *Akademik Fedorov* and RV *Professor Khljustin*, the routes of which covered the most part of the Northern Sea Route from the Barents to Japan Sea. The data obtained were used to analyze the optical and microphysical characteristics and chemical composition of aerosol of the Arctic Ocean and Far East seas. It should be noted that the results and regularities, discussed here, are estimative in character because of high spatiotemporal variations of atmospheric aerosol for relatively short periods of observations in separate regions. Like in other marine expeditions, the aerosol characteristics were determined by the specific features of hydrometeorological conditions in measurement periods, to some or another degree. At the same time, we underline the importance of acquiring the new information on specific features of physical-chemical aerosol composition in hard-to-reach and poorly studied regions of the planet.

The studies performed make it possible to draw the following main conclusions.

a. The atmospheric AOD in Siberian sector of Arctic and in the subpolar Bering Sea was characterized by small and nearly identical values: the average AOD values at the wavelength of 0.5 µm were 0.03; in particular, the finely dispersed component was 0.021, and the coarsely dispersed component was 0.009. For a comparison, we note that AOD values over Arctic seas turned out to be 5 times smaller than in background midlatitude regions, and a factor of 1.5–2 smaller than

ACPD
15, 16775–16859, 2015

in the region of Spitsbergen in this same time period. The high transparency of the atmosphere over the Arctic Ocean stemmed from the fact that there were no severe forest fires in the boreal part of Russia in that period. The growth in the southern direction is manifested in the spatial distribution of aerosol turbidity of the atmosphere over Far East seas. The AOD characteristics over the Bering Sea are almost the same as in Arctic; and AOD over the Japan Sea increases by more than a factor of 5 in the visible spectral range and by up to a factor of 3 in IR range.

b. The average boundary layer height (H_{BL}), measured by ship-based lidar in cruise of RV *Professor Khljustin*, was 520 m; and the maximal boundary layer height (near the Arctic port of Pevek) was 1200 m. In the latitudinal distribution, the height H_{BL} first decreased, and then increased northward of 55° N. The boundary layer height showed a similar distribution in CALIPSO satellite data, with a characteristic minimum at the latitude ~ 55° N. The elevated values of the height H_{BL} at subarctic latitudes seem to be due to increased effect of continent (Chukchi Peninsula) and predominating winds from the direction of the land. (The H_{BL} values are generally lower when air masses are carried from the direction of ocean.)

c. The local measurements of disperse composition of aerosol and concentration of black carbon in the near-ground layer showed their high variability even in the clean atmosphere of Arctic. Nonetheless, on the average, the aerosol and black carbon contents can be traced to decrease in the northeastern direction along the route of RV *Akademik Fedorov*. The largest average concentrations were observed in the southern part of the Barents Sea: $N_A = 6.5\,cm^{-3}$; $M_A = 1290\,ng\,m^{-3}$; and $M_{BC} = 140\,ng\,m^{-3}$. As the separation from the Kola Peninsula grew, the aerosol number and mass concentrations decreased on the average by 10–30 %, down to $N_A = 2.5$–$5.7\,cm^{-3}$ and $M_A = 830$–$930\,ng\,m^{-3}$. The differences in aerosol concentrations over other regions of the Arctic Ocean were mainly determined by the specific character of hydrometeorological conditions, and not by the degree of separation from the continent. A stronger and longer-term decrease (with increas-

ACPD
15, 16775–16859, 2015

ing distance from Scandinavian Peninsula) was found for the mass concentration of black carbon. The average M_{BC} value decreased by a factor of ~6 down to 22 ng m^{-3} in the northern part of the route (region A).

Comparison with data of our earlier studies in high-latitude regions (Polkin et al., 2011a; Sakerin et al., 2012) showed that the average particle volume distributions dV/dr vary in accordance with the degree of effect of continental aerosol outflows, and the total range of difference reaches two orders of magnitude. The maximal distributions dV/dr are characteristic for the subpolar White Sea, surrounded by land. Intermediate values of the particle concentrations in the entire size range were observed over the Kara Sea and on the Spitsbergen Archipelago; and the lowest values were observed in the Siberian sector of the Arctic Ocean. The small content of particles in this region is explained not only by remoteness from the sources of continental aerosol, but also by low temperatures and a weak generation of maritime aerosol from partially snow- and ice-covered surface.

d. As expected, the range of the spatiotemporal variations in aerosol and black carbon concentrations along the Far East route of RV *Professor Khljustin* (42–71° N) turned out to be much wider: N_A varied from 0.003 to 90.2 cm^{-3}; M_A varied from 1 to 13 630 ng m^{-3}; and M_{BC} varied from 2 to 400 ng m^{-3}. Averaging of aerosol parameters within four latitude zones, corresponding to separate seas, made it possible to identify the tendency toward their latitudinal decrease from south to north. The aerosol number concentration decreased from 23.7 cm^{-3} over the Japan Sea to 2.5 cm^{-3} over the Chukchi Sea (by about a factor of 9), the black carbon mass concentration decreased from 150 to 50 ng m^{-3} (by about a factor 3), and the aerosol mass concentration decreased by almost a factor of 4.

The obtained results indicate that the number concentrations of fine and coarse aerosols show opposite latitudinal variations; as a consequence, the relative contribution of coarsely dispersed fraction in Arctic zone increased by a factor of 4.5. This was favored not only by weakening of outflows of small-sized continental

ACPD
15, 16775–16859, 2015

aerosol, but also by increase in generation of large-sized maritime aerosol under the influence of strong wind and sea roughness at high latitudes. It is shown that, with respect to relative contents of two aerosol fractions, we can quite distinctly single out two zones: midlatitudes (southward of 64° N) where fine aerosol predominates and the mean ratio $(N_c/N_f) = 10^{-2}$; and Arctic latitudes where the role of large particles increases and the ratio (N_c/N_f) grows to 4.5×10^{-2}.

Based on analysis of aerosol number concentrations and meteorological parameters for the entire period of measurements, we obtained regression model (Eq. 5), which reflects the linear dependence of N_A on wind speed, air temperature, and rainfall amount. Good agreement between the actual and model-calculated N_A values is observed in the following range of meteorological conditions: wind speed $0.5 < WS < 10\,m\,s^{-1}$, air temperature $-2.5 < T < 16\,^{\circ}C$, and rainfall $0 < RF < 44\,mm\,h^{-1}$.

e. Based on results of the chemical analysis of samples, collected in cruise of RV *Akademik Fedorov*, for four regions of the Arctic Ocean we determined the average contents of ions and water-soluble elements in aerosol. The sodium ions and chloride ions predominated in aerosol composition throughout the route. The lowest ion content in aerosol was recorded over the Barents Sea, a factor of 2–3 smaller than in Siberian sector of Arctic. It was noted that ion-poor composition of aerosol (as well as elements and gaseous impurities) over the Barents Sea could stem from insufficient data confidence due to small number of aerosol samples.

We singled out three groups with respect to concentrations of water-soluble elements in aerosol composition. The main contribution (94 % of the total content) is made by elements of predominately terrigenous origin, i.e., Fe, Zn, Al, Ba, Cu, and Sr, with concentrations from several tens to several tenths of $ng\,m^{-3}$. The elements ranked second in significance for aerosol composition (5.6 %) are those of primarily anthropogenic origin (markers), i.e., Ni, Cd, Cr, Se, Pb, V, and Mo, with concentrations from several tens to several hundredths of $ng\,m^{-3}$. The smallest

ACPD
15, 16775–16859, 2015

(0.6 %) contribution to aerosol composition comes from elements of mixed origin (from natural and anthropogenic sources), namely, Ti, Co, Sb, Li, and As with concentrations from several thousandths to analytical zero. High intensity of aerosol enrichment by the elements Fe, Zn, Cu, Cd, and Cr is revealed for Siberian sector of Arctic.

Analysis of variations in the content of small gaseous impurities (HCl, HNO_3, SO_2, and NH_3) and variations in the sum of ions showed the presence of their interrelation with the correlation coefficient of 0.68. The vertical fluxes of water-soluble substances to marine surface are estimated. On the average, ions accounted for about 24.5 %, trace elements accounted for 0.4 %, and small gaseous impurities accounted for 75 % of the total amount of water-soluble substances arriving from the atmosphere.

f. We performed a chemical analysis of the atmospheric aerosol composition along the route of RV *Professor Khljustin* (Japan, Okhotsk, Bering, Chukchi, and East Siberian Seas). The ion content in aerosol varied in a wide range. The ion composition of aerosol differed both among separate seas, and in the same regions, between the forward and backward routes of the ship. A regularity of latitudinal variations in concentrations of ions and small gaseous impurities is recorded for the first half of the route. In particular, the total ion concentration decreased by 30 % as the vessel moved from low to high latitudes. No latitudinal dependence in the contents of ions and gaseous impurities is revealed on backward route of the ship, when sea surface roughness was stronger. The strongest effect of continental sources on aerosol composition was manifested in the first half of the cruise, especially in water basins of the Japan, Okhotsk, and East Siberian Seas, where the percentage of nss-Ca^{2+} reached 80–99 %.

Data averaging over three larger water basins (the Arctic Ocean and northern and southern Far East seas) showed that the average concentrations of most ions increase in the southern direction. As a result, the summed concentration of

ACPD
15, 16775–16859, 2015

ions, as compared to the Arctic Ocean, increased by 73 % over the Bering and Chukchi seas and by a factor of 2.5 at midlatitudes.

The percentage of water-soluble microelements over water basins of Far East seas varied from 0.1 to 25 % of the total number of inorganic components. The water-soluble elements were most abundant in aerosol, collected over the Okhotsk and Chukchi Seas. With respect to mass fraction in the aerosol composition, like in the cruise of RV *Akademik Fedorov*, we singled out three similar groups of elements. The maximal enrichment coefficients $(C_i/\mathrm{Na})_{\mathrm{aer}}/(C_i/\mathrm{Na})_{\mathrm{sw}}$, reaching 3–4 orders of magnitude, are found for Zn and Cr over water basins of Okhotsk and Chukchi Seas. The enrichment coefficients for Zn over other water basins were found to be 2–3 orders of magnitude. The maximal pollution by Cr compounds is found in the atmosphere of the Bering Sea.

We determined the average content of small gaseous impurities in the atmosphere for separate seas along the forward and backward routes. The variations in the SO_2 and MSA concentrations are found to be closely interrelated, with correlation coefficient of 0.77, possibly indicating that DMS was oxidized to give SO_2. Comparison with the data from Arctic cruise of *Akademik Fedorov* showed that the concentration of gaseous HCl was several times higher, while the SO_2 and NH_3 concentrations were several times lower, over Far East seas.

As in Arctic basin, the substances from the atmosphere to the water surface of Far East seas are supplied mainly together with gaseous impurities. Their relative contribution is 77–89 % of the total sum of water-soluble components. The deposited ions together with aerosol account for from 11 to 23 %, and trace elements account for 0.2–0.4 %. The vertical fluxes of substances from the atmosphere are found to be maximal (minimal) over the water basin of the Japan (East Siberian) Sea.

Acknowledgements. Authors thank the crews of RV *Akademik Fedorov* and *Professor Khljustin* for assistance and support in the expedition studies. For an opportunity to incorporate additional

ACPD
15, 16775–16859, 2015

information, which was used in our publication, we also gratefully acknowledge the scientific organizations such as:

- Tiksi meteorological observatory and GSFC/NASA for data of AERONET observations in the region of Tiksi;
- NOAA Air Resources Laboratory (ARL) for possibility to use HYSPLIT transport model (ECMWF Interim data);
- NASA/LaRC Science Data Center and the CALIPSO Search and Subsetting web application (https://www-calipso.larc.nasa.gov) for providing access to the CALIPSO data;
- IACP FEB RAS Multiple Access Center "Laser methods of investigating condensed media and biological objects and environmental monitoring" for providing access to experimental facilities.

This work was supported by the Program of Basic Research of Presidium of the Russian Academy of Sciences no. 23 and projects of partnership basic research of Siberian Branch of Russian Academy of Sciences no. 25. The results of planetary boundary layer investigations was funded by Russian Fund for Basic Research Grant No 14-50-00034 and Russian Science Foundation No 14-19-00589.

References

Albrecht, B.: Aerosols, cloud microphysics, and fractional cloudiness, Science, 245, 1227–1230, 1989.

Alekseev, G. V., Ivanov, N. E., Pnyushkov, A. V., and Kharlanenkova, N. E.: Climate change in the marine Arctic in the beginning of 21st century, in: Meteorological and Geophysical Researches, edited by: Alekseev, G. V., Paulsen, Moscow, Saint Petersburg, Russia, 352 pp., 2011 (in Russian).

Andreev, S. Y., Afonin, S. V., Bedareva, T. V., et al.: Study of radiative characteristics of aerosol in Asian part of Russia, edited by: Sakerin, S. M., Publishing House of Institute of Atmospheric Optics SB RAS, Tomsk, Russia, 484 pp., 2012 (in Russian).

Balin, Y. S., Ershov, A. D., and Penner, I. E.: Shipborne lidar investigations of aerosol fields in the atmosphere over Lake Baikal – Part 1: Longitudinal sections, Atmos. Ocean. Opt., 16, 402–410, 2003 (in Russian).

ACPD
15, 16775–16859, 2015

Behera, S. N., Sharma, M., Aneja, V. P., and Balasubramanian, R.: Ammonia in the atmosphere: a review on emission sources, atmospheric chemistry and deposition on terrestrial bodies, Environ. Sci. Pollut. R., 20, 8092–8131, doi:10.1007/s11356-013-2051-9, 2013.
Bigg, E. K., Grass, J. L., and Mossop, D. J. C.: Wind-produced submicron particles in the marine atmosphere, Atmos. Res., 36, 55–68, 1995.
Boé, J., Hall, A., and Qu, X.: Current GCMs' unrealistic negative feedback in the arctic, J. Climate, 22, 4682–4695, 2009.
Bradley, R. S. and Keimig, F. T.: Recent changes in the North American Arctic boundary layer in winter, J. Geophys. Res., 98, 8851–8858, 1993.
Bukin, O. A., Pavlov, A. N., Saluk, P. A., Kulchin, Y. N., Shmirko, K. A., Stolyarchuk, S. Y., and Bubnovskii, A. Y.: Peculiarities of the aerosol vertical distribution during the passage of dust storms over the Peter the Great Bay in 2006 and their influence on phytoplankton communities in the Japan Sea, Atmos. Ocean. Opt., 20, 306–312, 2007.
Bukin, O. A., Kulchin, Y. N., Pavlov, A. N., Stolyarchuk, S. Y., and Shmirko, K. A.: Characteristics of structure and dynamics of the planetary boundary layer in the transitional "ocean-continent" zone-Part 1: Winter period, Atm. Oceanic Opt., 26, 60–67, 2013.
Chubarova, N., Nezval', Ye., Sviridenkov, I., Smirnov, A., and Slutsker, I.: Smoke aerosol and its radiative effects during extreme fire event over Central Russia in summer 2010, Atmos. Meas. Tech., 5, 557–568, doi:10.5194/amt-5-557-2012, 2012.
Deser, C., Tomas, R., Alexander, M., and Lawrence, D.: The seasonal atmospheric response to projected Arctic sea ice loss in the late twenty-first century, J. Climate, 23, 333–351, 2010.
Dmitrenko, I. A., Kirillov, S. A., Tremblay, L. B., Kassens, H., Anisimov, O., Lavrov, S. A., Razumov, S. O., and Grigoriev, M. N.: Recent changes in shelf hydrography in the Siberian Arctic: potential for subsea permafrost instability, J. Geophys. Res.-Oceans, 116, C10027, doi:10.1029/2011JC007218, 2011.
Duce, R. A., Liss, P. S., Merrill, J. T., Atlas, E. L., Buat-Menard, P., Hicks, B. M., Miller, B. J., Prospero, R., Arimoto, J. M., Church, T. M., Ellis, W., Galloway, J. N., Hansen, L., Jickells, T. D., Knap, A. H., Reinhardt, K. H., Schneider, B., Soudine, A. J., Tokos, J., Tsunogai, S., Wollast, R., and Zhou, M.: The atmospheric input of trace species to the world ocean, Global Biogeochem. Cy., 5, 193–259, 1991.
Eck, T. F., Holben, B. N., Reid, J. S., Sinyuk, A., Hyer, E. J., O'Neill, N. T., Shaw, G. E., Vande Castle, J. R., Chapin, F. S., Dubovik, O., Smirnov, A., Vermote, E., Schafer, J. S., Giles, D., Slutsker, I., Sorokine, M., and Newcomb, W. W.: Optical properties of boreal region biomass

ACPD
15, 16775–16859, 2015

burning aerosols in central Alaska and seasonal variation of aerosol optical depth at an Arctic coastal site, J. Geophys. Res., 114, D11201, doi:10.1029/2008JD010870, 2009.
Eisenman, I., Untersteiner, N., and Wettlaufer, J. S.: On the reliability of simulated Arctic sea ice in global climate models, Geophys. Res. Lett., 34, L10501, doi:10.1029/2007GL029914, 2007.
EMEP: Manual for sampling and chemical analysis, Norwegian Institute for Air Research, EMEP/CCC-Report 1/95, O-7726, 176 pp. 1996.
Golobokova, L. P., Polkin, V. V., Kabanov, D. M., Khodzher, T. V., Terpugova, S. A., Chernov, D. G., Chipanina, E. V., Panchenko, M. V., and Sakerin, S. M.: Studies of atmospheric aerosol in the Arctic regions of Russia, Journal Ice and Snow/Led i Sneg, 122, 129–136, 2013 (in Russian).
Goryunova, N. V. and Shevchenko, V. P.: Study of aerosols and particulate matter in snow on drifting ice in the western part of the Russian Arctic in August–September 2006, Problems of the Arctic and Antarctic/Problemy Arktiki i Antarktiti, 78, 112–117, 2008 (in Russian).
Grimm, H. and Eatough, D. J.: Aerosol measurement: the use of optical light scattering for the determination of particulate size distribution, and particulate mass, including the semi-volatile fraction, J. Air Waste Manage., 59, 101–107, 2009.
Hansen, A. D. A., Polissar, A. V., and Schnell, R. C.: Airborne aerosol and black carbon measurements over the East Siberian Sea, spring 1992, Atmos. Res., 44, 153–165, 1997.
Haywood, J. and Boucher, O.: Estimates of the direct and indirect radiative forcing due to tropospheric aerosols: a review, Rev. Geophys., 38, 513–543, 2000.
Hennemuth, B. and Lammert, A.: Determination of the atmospheric boundary layer height from radiosonde and lidar backscatter, Bound.-Lay. Meteorol., 120, 181–200, 2006.
Herber, A., Thomason, L. W., Gernandt, H., Leiterer, U., Nagel, D., Schulz, K., Kaptur, J., Albrecht, T., and Notholt, J.: Continuous day and night aerosol optical depth observations in the Arctic between 1991 and 1999, J. Geophys. Res., 107, 4097, doi:10.1029/2001JD000536, 2002.
Holben, B. N., Eck, T. F., Slutsker, I., Tanre, D., Buis, J. P., Setzer, A., Vermote, E., Reagan, J. A., Kaufman, Y. J., Nakadjima, T., Lavenu, F., Jankowiak, I., and Smirnov, A.: AERONET – a federated instrument network and data archive for aerosol characterization, Remote Sens. Environ., 66, 1–16, 1998.
Hov, Ø., Shepson, P. B., and Wolff, E. W.: The chemical composition of the polar atmosphere – the IPY contribution, WMO Bull., 56, 263–270, 2007.

ACPD
15, 16775–16859, 2015

Huang, L., Gong, S. L., Sharma, S., Lavoué, D., and Jia, C. Q.: A trajectory analysis of atmospheric transport of black carbon aerosols to Canadian high Arctic in winter and spring (1990–2005), Atmos. Chem. Phys., 10, 5065–5073, doi:10.5194/acp-10-5065-2010, 2010.
ICS-3000 Ion Chromatography System Operator's Manual, Dionex Corporation, Document No. 065031., 392 pp., 2008.
IPCC 2007 Climate Change 2007: Synthesis Report, Intergovernmental Panel on Climate Change, 52 pp., available at: http://www.ipcc.ch/pdf/assessment-report/ar4/syr/ar4_syr.pdf (last access: 2012), 2007.
IPCC 2013 Climate Change 2013: The Physical Science Basis, Intergovernmental Panel on Climate Change, 1552 pp., available at: http://www.climatechange2013.org/images/report/WG1AR5_ALL_FINAL.pdf (last access: 2014), 2013.
Jacob, D. J.: Heterogeneous chemistry and tropospheric ozone, Atmos. Environ., 34, 2131–2159, 2000.
Johnson, B., Shine, K., and Forster, P.: The semi-direct aerosol effect: impact of absorping aerosols on marine stratocumulus, Q. J. Roy. Meteor. Soc., 130, 1407–1422, 2004.
Kabanov, D. M., Veretennikov, V. V., Voronina, Y. V., Sakerin, S. M., and Turchinovich, Y. S.: Information system for network sunphotometers, Atmos. Ocean. Opt., 22, 121–127, doi:10.1134/S1024856009010187, 2009.
Kay, J. E., Raeder, K., Gettelman, A., and Anderson, J.: The boundary layer response to recent arctic sea ice loss and implications for high-latitude climate feedbacks, J. Climate, 24, 428–447, 2011.
Kondratyev, K. Y.: Aerosol as a climate-forming component of the atmosphere. 2. Direct and indirect impact on climate, Atmos. Ocean. Opt., 15, 267–284, 2002.
Kondratyev, K. Y.: Aerosol and climate studies: current state and prospects. 3. Aerosol radiative forcing, Atmos. Ocean. Opt., 19, 505–513, 2006.
Kopeikin, V. M., Repina, I. A., Grechko, E. I., and Ogorodnikov, B. I.: Measurements of the soot aerosol content in the near-water layer in Southern and Northern Hemispheres, Atmos. Ocean. Opt., 23, 444–450, 2010 (in Russian).
Kozlov, V. S., Shmargunov, V. P., and Polkin V. V.: Spectrometers to study the properties of light absorption by aerosol particles, Instrum. Exp. Tech., 5, 155–157, 2008 (in Russian).
Kozlov, V. S., Polkin, V. V., Panchenko, M. V., Golobokova, L. P., Turchinovich Y. S., and Khodzher, T. V.: Results of integrated aerosol experiment in the continent-ocean transition zone (Primorye and the Sea of Japan). Part 3. Microphysical characteristics and ion compo-

ACPD
15, 16775–16859, 2015

sition of aerosol in the near-ground and near-water layers, Atmos. Ocean. Opt., 23, 967–977, 2010 (in Russian).
Kozlov, V. S., Yausheva, E. P., Terpugova, S. A., Panchenko, M. V., Chernov, D. G., and Shmargunov, V. P.: Optical–microphysical properties of smoke haze from Siberian forest fires in summer 2012, Int. J. Remote Sens., 35, 5722–5741, 2014.
Luangjame, J.: Recent Information of the EANET Network Center from the Editor, Eanet Science Bulletin, 3, 3–21, 2013.
Manual AZ-10: Research and Production Division "ECO-INTECH", Moscow, available at: http://www.eco-intech.com/img/AVimg/Brochure/AZ10.pdf (last access: 5 April 2014), 2010.
Menut, L., Flamant, C., Pelon, J., and Flamant, P. H.: Urban boundary-layer height determination from lidar measurements over the Paris area, Appl. Optics, 38, 945–954, 1999.
Menzies, R. T. and Tratt, D. M.: Airborne lidar observations of tropospheric aerosols during the Global Backscatter Experiment (GLOBE) Pacific circumnavigation missions of 1989 and 1990, J. Geophys. Res., 102, 3701–3714, 1997.
Nilsson, E. D.: Planetary boundary layer structure and airmass transport during the International Arctic Ocean Expedition 1991, Tellus B, 48, 178–196, 1996.
Nilsson, E. D., Rannik, U., Swietlicki, E., Leck, C., Aalto, P. P., Zhou, J., and Norman, M.: Turbulent aerosol fluxes over the Arctic Ocean. 2. Wind-driven sources from the sea, J. Geophys. Res., 106, 32139–32154, 2001.
O'Dowd, C. D. and Smith, M. H.: Physicochemical properties of aerosols over the northeast Atlantic: evidence for wind-speed-related submicron sea-salt aerosol production, J. Geophys. Res., 98, 1137–1149, 1993.
Pavlov, A. N., Shmirko, K. A., and Stolyarchuk, S. Y.: Characteristics of structure and dynamics of the planetary boundary layer in the "Ocean–Continent" zone – Part 2: Summer period, Atmos. Ocean. Opt., 26, 285–292, 2013.
Peters, T. M., Ott, D., and O'Shaughnessy, P. T.: Comparison of the Grimm 1.108 and 1.109 portable aerosol spectrometer to the TSI 3321 aerodynamic particle sizer for dry particles, Ann. Occup. Hyg., 50, 1–8, doi:10.1093/annhyg/mel067, 2013.
Petrenko, V. V., Ethiridge, D. M., Weiss, R. F., Brook, E. J., Shaefer, H., Severinghaus, J. P., Smith, A. M., Lowe, D., Hua, Q., and Riedel, K.: Methane from the East Siberian Arctic Shelf, Science, 329, 1146–1147, 2010.
Polkin, V. V., Panchenko, M. V., and Golobokova, L. P.: Ion composition of near-water aerosol over White Sea in Augusts of 2003–2006, Atmos. Ocean. Opt., 20, 911–916, 2007.

ACPD
15, 16775–16859, 2015

Polkin, V. V., Panchenko, M. V., Golobokova, L. P., Filippova, U. G., Khodzher, T. V., Lisitzin, A. P., and Shevchenko, V. P.: Aerosols in the marine boundary layer over the White and Kara seas in August–September 2007, in: Contribution of Russia to International Polar Year 2007/08. Meteorological and Geophysical Researches, Paulsen Editions, Moscow, Saint Petersburg, 199–214, 2011a (in Russian).

Polkin, V. V., Kozlov, V. S., Turchinovich, Y. S., and Shmargunov, V. P.: Comparative analysis of the microphysical characteristics of aerosol in the marine and coastal areas of Primorye, Atmos. Ocean. Opt., 24, 538–546, 2011b (in Russian).

Powell, K., Vaughan, M. A., Winker, D., Lee, K.-P., Pitts, M., and Trepte, C.: Cloud-Aerosol LIDAR Infrared Pathfinder Satellite Observations. Data Management System. Data Products Catalog, National Aeronautics and Space Administration, Langley Research Center, Hampton, Virginia, USA, 23681-2199, 122, 2013.

Radionov, V. F. and Marshunova, M. S.: Long-term variations in the turbidity of the Arctic atmosphere in Russia, Atmos. Ocean, 30, 531–549, 1992.

Radionov, V. F., Marshunova, M. S., Rusina, E. N., Lubo-Lesnichenko, K. E., and Pimanova, Y. E.: Atmospheric aerosol turbidity in polar regions, Izv. Atmos. Ocean. Phy., 30, 797–801, 1994 (in Russian).

Rahn, K. A.: Relative importances of North America and Eurasia as sources of Arctic aerosol, Atmos. Environ., 15, 1447–1455, 1981.

Rasool, S. I.: Chemistry of the Lower Atmosphere, Plenum Press, New York, USA, London, UK, 335 pp., 1973.

Redington, A. L. and Derwent, R. G.: Calculation of sulphate and nitrate aerosol concentrations over Europe using a Lagrangian dispersion model, Atmos. Environ., 36, 4425–4439, 2002.

Reist, P. C.: Aerosol Scienc and Technology, 2nd edn., McGraw-Hill, New York, USA, 379 pp., 1993.

Rudis, D. D.: Alaska Maritime National Wildlife Refuge – Bering Sea Unit Contaminant Assessment, U.S. Fish and Wildlife Service, Juneau Field Office, Alaska, 56 pp., 2010.

Sakerin, S. M. and Kabanov, D. M.: Spatial inhomogeneities and the spectral behavior of atmospheric aerosol optical depth over the Atlantic Ocean, J. Atmos. Sci., 59, 484–500, 2002.

Sakerin, S. M., Kabanov, D. M., Panchenko, M. V., Polkin, V. V., Holben, B. N., Smirnov, A. V., Beresnev, S. A., Gorda, S. Y., Kornienko, G. I., Nikolashkin, S. V., Poddubnyi, V. A., and Tashchilin, M. A.: Monitoring of atmospheric aerosol in the Asian part of Russia in 2004 within the framework of AEROSIBNET program, Atmos. Ocean. Opt., 18, 871–878, 2005.

ACPD
15, 16775–16859, 2015

Sakerin, S. M., Kabanov, D. M., Smirnov, A. V., and Holben, B. N.: Aerosol optical depth of the atmosphere over ocean in the wavelength range 0.37–4 µm, Int. J. Remote Sens., 29, 2519–2547, doi:10.1080/01431160701767492, 2008.

Sakerin, S. M., Chernov, D. G., Kabanov, D. M., Kozlov, V. S., Panchenko, M. V., Polkin, V. V., and Radionov, V. F.: Preliminary results of studying the aerosol characteristics of the atmosphere in the region of Barentsburg, Spitsbergen, Problemy Arktiki i Antarktiki, 1, 20–31, 2012 (in Russian).

Sakerin, S. M., Kabanov, D. M., Rostov, A. P., Turchinovich, S. A., and Knyazev, V. V.: Sun Photometers for measuring spectral air transparency in stationary and mobile conditions, Atmos. Ocean. Opt., 26, 352–356, 2013.

Sakerin, S. M., Andreev, S. Y., Kabanov, D. M., Nikolashkin, S. V., Prahov, A. N., Radionov, V. F., Turchinovich, Y. S., Chernov, D. G., Holben, B. N., Smirnov, A., and Sorokin, M. G.: On results of studies of atmospheric aerosol optical depth in Arctic regions, Atmos. Ocean. Opt., 27, 413–423, 2014 (in Russian).

Sasakawa, M., Shimoyama, K., Machida, T., Tsuda, N., Suto, H., Arshinov, M., Davydov, D., Fofonov, A., Krasnov, O., Saeki, T., Koyama, Y., and Maksyutov, S.: Continuous measurements of methane from a tower network over Siberia, Tellus, 62, 403–416, 2010.

Shakhova, N., Semiletov, I., Salyuk, A., Yusupov, V., Kosmach, D., and Gustafsson, Ö.: Extensive methane venting to the atmosphere from sediments of the East Siberian Arctic Shelf, Science, 327, 1246–1250, 2010.

Sharma, S., Lavoue, D., Cachier, H., Barrie, L. A., and Gong, S. L.: Long-term trends of the black carbon concentrations in the Canadian Arctic, J. Geophys. Res., 109, D15203, doi:10.1029/2003JD004331, 2004.

Shevchenko, V. P.: The influence of aerosols on the oceanic sedimentation and environmental conditions in the Arctic, Publishing House “Nauka”, Moscow, Russia, 226 pp., 2006 (in Russian).

Shevchenko, V. P., Lisitsin, A. P., Vinogradova, A. A., Smirnov, V. V., Serova, V. V., and Stein, R.: Arctic aerosols. Results of ten-year investigations, Atmos. Ocean. Opt., 13, 510–533, 2000.

Shmirko, K. A., Pavlov, A. N., Stolyarchuk, S. Y., Salyuk, P. A., and Bukin, O. A.: Radiative components dynamics at the Far East region, Proceedings of SPIE, 7860, Lidar Remote Sensing for Environmental Monitoring XI, 78600S (11 November 2010), doi:10.1117/12.869619, 2010.

ACPD
15, 16775–16859, 2015

Shmirko, K. A., Pavlov, A. N., Stolyarchuk, S. Y., Mayor, A. Y., and Bukin, O. A.: Typical patterns of PBL structure and dynamics in transitional ocean-continent zone in summer and winter in Far East region, Proceedings of SPIE, 8526, Lidar Remote Sensing for Environmental Monitoring XIII, 85260U (19 November 2012), doi:10.1117/12.977387, 2012.

Smirnov, V. V., Savchenko, A. V., Pronin, A. A., Kuusk, V. V., and Radionov, V. F.: Variability in aerosol and air ion composition in the Arctic spring, Atmos. Res., 49, 163–176, 1998.

Stohl, A., Andrews, E., Burkhart, J. F., Forster, C., Herber, A., Hoch, S. W., Kowal, D., Lunder, C., Mefford, T., Ogren, J. A., Sharma, S., Spichtinger, N., Stebel, K., Stone, R., Ström, J., Tørseth, K., Wehrli, C., and Yttri, K. E.: Pan-Arctic enhancements of light absorbing aerosol concentrations due to North American boreal forest fires during summer 2004, J. Geophys. Res., 111, D22214, doi:10.1029/2006JD007216, 2006.

Tomasi, C., Vitale, V., Lupi, A., Di Carmine, C., Campanelli, M., Herber, A., Treffeisen, R., Stone, R. S., Andrews, E., Sharma, S., Radionov, V. F., von Hoyningen-Huene, W., Stebel, R., Yansen, G. H., Myhre, C. L., Wehrli, C., Aaltonen, V., Lihavainen, Y., Virkkula, A., Hillamo, R., Ström, J., Toledano, C., Cachorro, V. E., Ortiz, P., de Frutos, A. M., Blindheim, S., Frioud, M., Gausa, M., Zeielinski, T., Petelski, T., and Yamanouchi, T.: Aerosol in polar regions: a historical overview based on optical depth and in situ observations, J. Geophys. Res., 112, D16205, doi:10.1029/2007JD008432, 2007.

Tomasi, C., Lupi, A., Mazzola, M., Stone, R. S., Dutton, E. G., Herber, A., Radionov, V. F., Holben, B., Sorokin, M., Sakerin, S. M., Terpugova, S. A., Lanconelli, C., Petkov, B., and Vitale, V.: An update of the long-term trend of aerosol optical depth in the polar regions using POLAR-AOD measurements performed during International Polar Year, Atmos. Environ., 52, 29–47, 2012.

Toyama, K., Zhang, J., and Satake, H.: Long-range transportation and deposition of chemical substances over the Northern Japan Alps mountainous area, Geochem. J., 47, 683–692, 2013.

Troen, I. and Mahrt, L.: A simple model of the atmospheric boundary layer: Sensitivity to surface evaporation, Bound.-Lay. Meteorol., 37, 129–148, 1986.

Tsunogai, S., Saito, O., Yamada, K., and Nakay, S.: Chemical composition of oceanic aerosol, J. Geophys. Res., 77, 5283–5292, 1972.

Turekian, K. K.: Oceans, Foundations of Earth Science Series, Prentice Hall, Englewood Cliffs, USA, 120 pp., 1968.

ACPD
15, 16775–16859, 2015

Twomey, S.: The influence of pollution on the shortwave albedo of clouds, J. Atmos. Sci., 34, 1149–1152, 1977.
Vinogradova, A. A.: Seasonal and long-term variations in atmospheric circulation indices and air mass transport to the Russian Arctic, Atmos. Ocean. Opt., 27, 463–472, 2014 (in Russian).
Vinogradova, A. A. and Ponomareva, T. Y.: Sources and sinks of anthropogenic microelements in the Arctic atmosphere: tendencies in variations from 1981 to 2005, Atmos. Ocean. Opt., 20, 433–441, 2007.
Vinogradova, A. A. and Veremeichik, A. O.: Model estimates of anthropogenic black carbon concentration in the Russian Arctic atmosphere, Atmos. Ocean. Opt., 26, 443–451, 2013 (in Russian).
Vogelezang, D. H. P. and Holtslag, A. A. M.: Evaluation and model impacts of alternative boundary-layer height formulations, Bound.-Lay. Meteorol., 81, 245–269, 1996.
Wang, Q. and Wang, S.: Turbulent and thermodynamic structure of the autumnal Arctic boundary layer due to embedded clouds, Bound.-Lay. Meteorol., 113, 225–247, 2004.
Wang, Q., Jacob, D. J., Fisher, J. A., Mao, J., Leibensperger, E. M., Carouge, C. C., Le Sager, P., Kondo, Y., Jimenez, J. L., Cubison, M. J., and Doherty, S. J.: Sources of carbonaceous aerosols and deposited black carbon in the Arctic in winter-spring: implications for radiative forcing, Atmos. Chem. Phys., 11, 12453–12473, doi:10.5194/acp-11-12453-2011, 2011.
Zilitinkevich, S. and Esau, I.: Planetary boundary layer feedbacks in climate system and triggering global warming in the night, in winter and at high latitudes, Geography, Environment, Sustainability, 1, 20–34, 2009.

ACPD
15, 16775–16859, 2015

Table 1. Brief characteristics of instruments in aerosol complex.

Instruments	Main characteristics	
	RV *Akademik Fedorov*	RV *Professor Khljustin*
SPM sun photometers	AOD and water vapor content of the atmosphere with uncertainties of 0.01–0.02 and 0.1 g cm^{-2}, respectively. Field of view angle is 1.5–2.5°. Passband maxima of filters are at: 381, 373, 405, 500, 550, 673, 775, 870, 933, 1045, 1249, 2132 nm	341, 367, 439, 501, 547, 676, 777, 871, 938, 1044, 1553, 2136 nm
Particle counters	GRIMM 1.108. Particle number and mass concentrations in 15 size ranges from 0.3 to 20 µm: 0.3–0.4; 0.4–0.5; 0.5–0.65; 0.65–0.8; 0.8–1.0; 1.0–1.6; 1.6–2.0; 2.0–3.0; 3.0–4.0; 4.0–5.0; 5.0–7.5; 7.5–10; 10–15; 15–20 µm. Tolerance Ranges: count correlation at 1 µm ±5 %; relative mass deviation ±5 % to reference unit.	AZ-10. Particle number and mass concentrations in 6 diameter ranges from 0.3 to 10 µm: 0.3–0.4; 0.4–0.5; 0.5–1.0; 1.0–2.0; 2.0–5.0; 5.0–10 µm. Tolerance Ranges: ±30 %.
Aethalometers (Kozlov et al., 2008)	Mass concentration of black carbon in particles of submicron range. Sensitivity is 10 ng m^{-3}.	

ACPD
15, 16775–16859, 2015

Table 2. Geographic positions of regions and periods of sun photometer measurements.

Area no.	Geographic characteristic	Latitude	Longitude	Time
1	Barentsburg (Spitsbergen archipelago)	78° N	14° E	21 Aug–7 Sep
2	Northeastern margin of Kara Sea	82° N	98° E	14 Sep
3	Polyarka (Tiksi) – coast of Laptev Sea	72° N	129° E	26 Aug–21 Sep
4	Northeastern margin of Laptev Sea	80° N	150° E	2 Sep
5	De Long Strait – Chukchi Sea	69° N	179° W	13 Aug
6	Bering Sea (along coasts of Russia)	60° N	170° E	4, 26–28 Sep
7	Near Pacific coast of Kamchatka	52° N	159° E	31 Jul, 1–3 Sep
8	Vladivostok – coast of Japan Sea	43° N	132° E	27 Jul–6 Sep

ACPD
15, 16775–16859, 2015

Table 3. Average characteristics of AOD and water vapor content in Arctic and Far East seas (the geographic positions of regions 1–8 are presented in Fig. 1 and in Table 2).

Characteristics	Arctic regions						Far East Seas		
	1	2	3	4	5	< 2–5 >	6	7	8
$\tau^{a}_{0.37}$	0.078	0.041	0.056	0.031	0.044	0.043	0.043	0.096	0.242
$\tau^{a}_{0.5}$	0.053	0.029	0.038	0.026	0.028	0.030	0.033	0.058	0.186
$\tau^{a}_{0.87}$	0.030	0.016	0.015	0.019	0.014	0.016	0.023	0.034	0.101
$\tau^{a}_{2.14}$	0.023	0.013	–	0.014	0.009	0.012	0.016	0.022	0.044
α	1.06	1.17	1.72	0.52	1.26	–	0.67	0.85	1.04
β	0.026	0.013	0.011	0.018	0.012	–	0.021	0.031	0.089
$\tau^{f}_{0.5}$	0.030	0.020	0.033	0.012	0.020	0.021	0.018	0.037	0.142
τ^{c}	0.023	0.011	0.006	0.012	0.008	0.009	0.015	0.022	0.044
w	1.11	0.74	0.92	0.87	0.61	0.79	0.80	1.03	2.83

ACPD
15, 16775–16859, 2015

Table 4. Statistical characteristics of near-water aerosol in Arctic seas: numerator indicates mean and standard deviation (±SD); and denominator indicates the minimum (min) and maximum (max) values and the number of days of measurements (n).

Region and period of measurements	N_A, cm^{-3} mean±SD / min/max (n)	M_A, $ng\,m^{-3}$ mean±SD / min/max (n)	M_{BC}, $ng\,m^{-3}$ mean±SD / min/max (n)
K. Barents Sea near Kola Peninsula coasts (68–71° N, 18–21 Aug, RV *Akademik Fedorov*)	6.52±1.77 / 5.39–8.56 (3)	1290±70 / 1260/1360 (3)	140±100 / 80/250 (3)
B. Barents Sea (71–81° N, 21–23 Aug and 19–21 Sep, RV *Akademik Fedorov*)	5.55±1.08 / 4.83–7.44 (5)	930±230 / 710/1250 (5)	60±20 / 30/80 (6)
A. Arctic Ocean (77–84° N, 24 Aug–18 Sep, RV *Akademik Fedorov*)	5.76±2.92 / 2.02–11.9 (25)	880±540 / 230/2610 (25)	20±10 / 10/50 (26)
F. Chukchi and East Siberian Seas (69–71° N, 9–24 Aug, RV *Professor Khljustin*)	2.5±1.5 / 0.260–4.30 (14)	830±680 / 670/2320 (14)	50±20 / 20/90 (15)

ACPD
15, 16775–16859, 2015

Table 5. Statistical characteristics of aerosol in Far East seas: numerator indicates mean and standard deviation (±SD); and denominator indicates the minimum (min), maximum (max) values and the number of measurement days (n).

Area	N_A, cm^{-3}	M_A, $ng\,m^{-3}$	M_{BC}, $ng\,m^{-3}$
Japan Sea, 42–46.5° N	23.6±15.1 / 9.66–57.9 (8)	2970±2380 / 840/6870 (8)	150±100 / 50/310 (6)
Okhotsk Sea, 46.5–52° N	9.4±10.2 / 0.687–25.5 (8)	1310±2220 / 40/6570 (8)	100±100 / 30/310 (8)
Bering Sea, 52–67° N	3.6±4.1 / 0.117–15.9 (18)	750±760 / 10/2640 (18)	60±30 / 10/100 (18)
Chukchi and East Siberian Seas, 67–71° N	2.5±1.5 / 0.260–4.30 (14)	830±680 / 670/2320 (14)	50±20 / 20/100 (15)

ACPD
15, 16775–16859, 2015

Table 6. Average characteristics of ion composition of atmospheric aerosol on the route of RV *Akademik Fedorov* in August–September 2013 (numerator indicates the average ion content in $\mu g\,m^{-3}$ and standard deviations; denominator indicates the minimum and maximum values, n is the number of samples; and $\sum_{ions}$ is the summed ion content).

Ions	Area				
	B (n = 2)	A_1 (n = 6)	A_2 (n = 4)	A_3 (n = 4)	A (n = 14)
Na^+	0.15±0.08 0.09–0.20	0.26±0.23 0.11–0.45	0.51±0.33 0.18–0.96	0.29±0.23 0.09–0.61	0.34 ± 0.24
NH_4^+	0.03±0.04 0.00–0.06	0.17±0.04 0.11–0.25	0.09±0.06 0.06–0.18	0.10±0.09 0.03–0.33	0.13 ± 0.07
K^+	0.07±0.09 0.00–0.13	0.05±0.09 0.00–0.23	0.04±0.04 0.02–0.11	0.04±0.03 0.01–0.07	0.04 ± 0.06
Mg^{2+}	0.01±0.00 0.00–0.01	0.02±0.01 0.01–0.04	0.04±0.02 0.03–0.07	0.03±0.03 0.00–0.07	0.03 ± 0.02
Ca^{2+}	0.01±0.01 0.01–0.02	0.03±0.02 0.02–0.07	0.04±0.02 0.03–0.06	0.04±0.02 0.00–0.07	0.04 ± 0.02
Cl^-	0.29±0.24 0.11–0.46	0.61±0.29 0.33–1.15	0.79±0.44 0.33–1.33	0.61±0.44 0.12–1.15	0.66 ± 0.36
NO_3^-	0.001±0.001 0.000–0.001	0.013±0.030 0.000–0.075	0.047±0.043 0.002–0.092	0.025±0.046 0.002–0.094	0.03 ± 0.04
SO_4^{2-}	0.05±0.00 0.05	0.10±0.02 0.08–0.13	0.15±0.10 0.05–0.28	0.09±0.08 0.01–0.21	0.11 ± 0.07
$\sum_{ions}$	0.61±0.46 0.27–0.93	1.25±0.64 0.83–2.06	1.71±0.88 0.73–2.86	1.22±0.78 0.30–2.19	1.38 ± 0.75

ACPD
15, 16775–16859, 2015

Table 7. Average values (±SD) of concentrations [ng m^{-3}] of water-soluble elements in aerosol along the route of RV *Akademik Fedorov* (August–September 2013).

Element	Area				
	B	A_1	A_2	A_3	A
Fe	2.60 ± 1.21	7.07 ± 4.21	2.99 ± 1.30	8.14 ± 5.23	6.06 ± 4.22
Zn	6.21 ± 4.19	7.99 ± 3.62	8.26 ± 4.53	10.51 ± 7.48	8.71 ± 4.81
Al	0.73 ± 1.03	0.73 ± 1.68	0.74 ± 1.39	0.59 ± 0.77	0.70 ± 1.33
Cu	0.76 ± 0.40	1.21 ± 0.97	0.85 ± 0.40	1.13 ± 0.57	1.08 ± 0.72
Sr	0.21 ± 0.11	0.61 ± 0.32	0.82 ± 0.48	0.51 ± 0.36	0.65 ± 0.38
Ba	1.34 ± 0.59	0.95 ± 0.60	1.03 ± 0.24	1.02 ± 0.42	0.99 ± 0.44
Ni	0.24 ± 0.24	0.32 ± 0.33	0.20 ± 0.23	0.26 ± 0.12	0.27 ± 0.25
Cd	0.20 ± 0.12	0.39 ± 0.21	0.27 ± 0.18	0.43 ± 0.16	0.36 ± 0.19
Cr	0.12 ± 0.17	0.076 ± 0.046	0.083 ± 0.083	0.16 ± 0.08	0.100 ± 0.074
Se	0.065 ± 0.091	0.14 ± 0.05	0.14 ± 0.05	0.15 ± 0.12	0.141 ± 0.068
Pb	0.056 ± 0.018	0.079 ± 0.029	0.101 ± 0.057	0.080 ± 0.025	0.086 ± 0.038
V	0.027 ± 0.021	0.025 ± 0.010	0.023 ± 0.007	0.025 ± 0.017	0.024 ± 0.010
Mo	0.036 ± 0.027	0.050 ± 0.021	0.038 ± 0.013	0.053 ± 0.025	0.047 ± 0.019
Ti	0.007 ± 0.004	0.122 ± 0.286	0.013 ± 0.030	0.028 ± 0.028	0.064 ± 0.189
Co	0.003 ± 0.005	0.0001 ± 0.0003	0.00	0.013 ± 0.026	0.003 ± 0.013
Sb	0.00	0.0015 ± 0.0040	0.045 ± 0.045	0.44 ± 0.88	0.126 ± 0.438
Li	0.00	0.0040 ± 0.0076	0.0093 ± 0.0101	0.0009 ± 0.0018	0.0049 ± 0.0079
As	0.0058 ± 0.0004	0.0079 ± 0.0036	0.0032 ± 0.0044	0.0056 ± 0.0041	0.0057 ± 0.0042
Be	0.00	0.00	0.00	0.00	0.00

ACPD
15, 16775–16859, 2015

Table 8. Average content of small gaseous impurities in the Arctic atmosphere according to measurements in August–September 2013 onboard RV *Akademik Fedorov* (numerator indicates the average values in $\mu g\,m^{-3}$ and standard deviations, denominator indicates the minimum and maximum values, and *n* is the number of samples).

Area	HCl	HNO_3	SO_2	NH_3
B	$\frac{0.51\pm0.04}{0.48–0.54}$	$\frac{0.30\pm0.12}{0.22–0.38}$	$\frac{2.92\pm3.30}{0.59–5.26}$	$\frac{0.55\pm0.11}{0.48–0.63}$
A_1	$\frac{0.74\pm0.34}{0.49–1.36}$	$\frac{0.44\pm0.14}{0.30–0.66}$	$\frac{5.23\pm2.40}{1.77–8.12}$	$\frac{0.86\pm0.36}{0.26–1.32}$
A_2	$\frac{1.09\pm0.49}{0.29–1.48}$	$\frac{0.55\pm0.13}{0.38–0.74}$	$\frac{3.11\pm2.64}{0.22–6.16}$	$\frac{0.63\pm0.15}{0.42–0.80}$
A_3	$\frac{1.00\pm0.78}{0.43–1.86}$	$\frac{0.38\pm0.31}{0.11–0.62}$	$\frac{4.20\pm23.31}{1.41–7.75}$	$\frac{0.63\pm0.60}{0.44–0.78}$
A	0.91 ± 0.46	0.46 ± 0.16	4.31 ± 2.55	0.73 ± 0.28

ACPD
15, 16775–16859, 2015

Table 9. Diurnally average vertical fluxes of water-soluble substances together with aerosol and gaseous impurities [mg m^{-2} day^{-1}] according to data of measurements in Arctic and Far East seas (RV *Akademik Fedorov* and RV *Professor Khljustin*).

Area	Deposition velocity								
	Ions	TE	GI	Ions	TE	GI	Ions	TE	GI
	3.4×10^{-4} m s^{-1}			1.9×10^{-3} m s^{-1}			2×10^{-2} m s^{-1}		
	Arctic seas								
Barents Sea (region B)	0.015	0.0004	0.07	0.09	0.002	0.41	0.91	0.022	4.28
Arctic ocean (region A)	0.041	0.0006	0.11	0.23	0.003	0.60	2.41	0.034	6.37
White Sea (Polkin et al., 2006)	0.34	–	0.26	1.88	–	1.45	19.8	–	15.3
Kara Sea (Polkin et al., 2011)	0.23	–	0.34	1.29	–	1.89	13.6	–	19.9
	Far East seas								
Japan Sea	0.078	0.0018	0.62	0.44	0.010	3.45	4.61	0.104	36.27
Okhotsk Sea	0.097	0.0016	0.48	0.54	0.009	2.68	5.70	0.093	28.19
Bering Sea	0.070	0.0007	0.28	0.39	0.004	1.55	4.15	0.043	16.27
Chukchi Sea	0.051	0.0009	0.17	0.28	0.005	0.96	2.99	0.055	10.13
East Siberian Sea	0.030	0.0005	0.15	0.17	0.003	0.85	1.78	0.030	8.92

ACPD
15, 16775–16859, 2015

Table 10. Diurnally average vertical fluxes of sulfur and nitrogen together with aerosol and gaseous impurities [mg m^{-2} day^{-1}] according to data of measurements in Arctic and Far East seas (RV *Akademik Fedorov* and RV *Professor Khljustin*).

Area	Deposition velocity											
	S_{aer}	N_{aer}	S_{gas}	N_{gas}	S_{aer}	N_{aer}	S_{gas}	N_{gas}	S_{aer}	N_{aer}	S_{gas}	N_{gas}
	3.4×10^{-4} m s^{-1}				1.9×10^{-3} m s^{-1}				2×10^{-2} m s^{-1}			
Arctic seas												
Barents Sea (B)	0.0007	0.0005	0.015	0.043	0.004	0.003	0.086	0.240	0.04	0.03	0.90	2.53
Arctic Ocean (A)	0.0029	0.0011	0.020	0.062	0.016	0.006	0.112	0.343	0.17	0.06	1.18	3.61
Far East seas												
Japan Sea	0.006	0.0019	0.0007	0.019	0.032	0.010	0.004	0.105	0.34	0.110	0.042	1.11
Okhotsk Sea	0.004	0.0003	0.0007	0.014	0.023	0.002	0.004	0.076	0.24	0.016	0.039	0.80
Bering Sea	0.008	0.0004	0.0006	0.004	0.046	0.002	0.003	0.024	0.48	0.025	0.034	0.25
Chukchi Sea	0.003	0.00	0.0017	0.003	0.014	0.00	0.010	0.018	0.15	0.003	0.103	0.19
East Siberian Sea	0.001	0.00	0.0011	0.002	0.004	0.00	0.006	0.010	0.04	0.001	0.067	0.10

ACPD
15, 16775–16859, 2015

Table 11. Average ion content (±SD) in μg m^{-3} in the atmosphere of Far East seas according to data of measurements onboard RV *Professor Khljustin* in July–September 2013 when the ship moved in the forward (shown in numerator) and backward (shown in denominator) directions, and *n* is the number of samples.

Ions	Area				
	Japan Sea *n* (4/1)	Okhotsk Sea *n* (3/2)	Bering Sea *n* (3/4)	Chukchi Sea *n* (6/2)	East Siberian Sea *n* (1/1)
Na^+	0.49±0.19 / 1.30	0.34±0.44 / 1.99±2.73	0.38±0.19 / 0.80±0.80	0.29±0.21 / 1.58±2.00	0.18 / 2.28
NH_4^+	0.05±0.01 / 0.04	0.02±0.02 / 0.00	0.01±0.01 / 0.02±0.02	0.00 / 0.00	0.00 / 0.00
K^+	0.45±0.21 / 0.61	0.39±0.55 / 0.11±0.11	0.06±0.02 / 0.41±0.52	0.04±0.03 / 0.19±0.23	0.10 / 0.11
Mg^{2+}	0.05±0.02 / 0.07	0.03±0.03 / 0.28±0.39	0.04±0.02 / 0.08±0.06	0.03±0.03 / 0.18±0.22	0.02 / 0.29
Ca^{2+}	0.13±0.06 / 0.10	0.10±0.10 / 0.11±0.13	0.03±0.01 / 0.10±0.06	0.03±0.01 / 0.10±0.12	0.04 / 0.14
Cl^-	0.82±0.27 / 2.23	0.58±0.64 / 3.21±4.18	0.66±0.42 / 1.41±1.47	0.53±0.40 / 1.60±1.80	0.31 / 4.25
Br^-	0.004±0.005 / 0.003	0.001±0.001 / 0.011±0.016	0.001±0.001 / 0.003±0.002	0.001±0.001 / 0.006±0.008	0.001 / 0.009
NO_3^-	0.10±0.10 / 0.14	0.00 / 0.01±0.02	0.00 / 0.02±0.02	0.01±0.01 / 0.00	0.00 / 0.00
SO_4^{2-}	0.66±0.13 / 0.28	0.29±0.19 / 0.61±0.82	0.34±0.31 / 1.22±1.03	0.13±0.06 / 0.60±0.71	0.07 / 0.67
$\sum_{ions}$	2.75±0.72 / 4.67	1.75±1.91 / 6.33±8.39	1.52±0.38 / 4.06±1.97	1.06±0.69 / 4.26±5.09	0.72 / 7.75

ACPD
15, 16775–16859, 2015

Table 12. Average values (±SD) of concentrations [ng m^{-3}] of water-soluble elements in aerosol composition over Far East seas (*Professor Khljustin*, July–September 2013).

Element	Area				
	Japan Sea	Okhotsk Sea	Bering Sea	Chukchi Sea	East Siberian Sea
Fe	6.1 ± 5.0	2.6 ± 3.1	2.0 ± 1.0	2.1 ± 1.5	0.55 ± 0.061
Zn	36.1 ± 11.6	35.5 ± 31.4	11.0 ± 2.1	20.3 ± 13.7	10.3 ± 5.8
Al	2.2 ± 0.8	5.6 ± 6.7	5.1 ± 7.2	1.6 ± 2.3	0.29 ± 0.032
Cu	8.1 ± 3.1	5.2 ± 5.2	3.9 ± 2.1	2.9 ± 1.1	3.0 ± 1.6
Sr	1.03 ± 0.31	1.10 ± 1.29	0.64 ± 0.54	0.61 ± 0.74	1.06 ± 0.72
Ba	2.1 ± 0.3	0.97 ± 0.50	1.0 ± 0.3	1.0 ± 0.4	1.05 ± 0.076
Ni	0.98 ± 0.46	0.41 ± 0.51	0.32 ± 0.35	0.62 ± 1.13	0.21 ± 0.08
Cd	0.11 ± 0.06	0.09 ± 0.05	0.14 ± 0.21	0.074 ± 0.029	0.050 ± 0.030
Cr	0.24 ± 0.06	0.14 ± 0.13	0.37 ± 0.41	0.078 ± 0.076	0.031 ± 0.031
Se	0.22 ± 0.14	0.06 ± 0.08	0.050 ± 0.078	0.10 ± 0.13	0.23 ± 0.07
Pb	0.41 ± 0.12	0.28 ± 0.23	0.25 ± 0.16	0.22 ± 0.06	0.16 ± 0.03
V	0.74 ± 0.67	0.16 ± 0.17	0.093 ± 0.069	1.22 ± 2.84	0.15 ± 0.03
Mo	0.039 ± 0.025	0.023 ± 0.024	0.016 ± 0.016	0.023 ± 0.014	0.024 ± 0.010
Ti	0.026 ± 0.036	0.00	0.003 ± 0.007	0.009 ± 0.023	0.00
Co	0.015 ± 0.011	0.007 ± 0.010	0.002 ± 0.006	0.005 ± 0.010	0.007 ± 0.010
Sb	0.065 ± 0.049	0.046 ± 0.048	0.013 ± 0.004	0.023 ± 0.016	0.014 ± 0.001
Li	0.077 ± 0.037	0.040 ± 0.040	0.023 ± 0.022	0.049 ± 0.053	0.044 ± 0.041
As	0.034 ± 0.035	0.023 ± 0.042	0.005 ± 0.012	0.012 ± 0.017	0.014 ± 0.013
Be	0.0002 ± 0.0003	0.0002 ± 0.0004	0.0001 ± 0.0002	0.0002 ± 0.0005	0.0012 ± 0.0021
Mn	1.51 ± 1.71	1.40 ± 1.99	0.11 ± 0.16	1.19 ± 1.04	0.20 ± 0.18

ACPD
15, 16775–16859, 2015

Table 13. The average concentrations of small gaseous impurities in the atmosphere [$\mu g\,m^{-3}$] over Far East seas (RV *Professor Khljustin*, July–September 2013) when the ship moved in the forward (given in numerator) and backward (given in denominator) directions.

Area	HCl	HNO_3	SO_2	NH_3
Japan Sea	24.51±10.92 / 6.41	0.56±0.42 / 0.01	0.81±0.18 / 0.05	0.05±0.03 / 0.03
Okhotsk Sea	24.69±2.66 / 3.62±0.83	0.66±0.06 / 0.00±0.00	0.70±0.28 / 0.09±0.10	0.03±0.05 / 0.03±0.04
Bering Sea	15.72±4.52 / 4.85±2.10	0.26±0.23 / 0.00±0.00	0.26±0.20 / 0.07±0.04	0.03±0.01 / 0.04±0.02
Chukchi Sea	6.26±3.43 / 4.61±4.71	0.00±0.00 / 0.00±0.00	0.11±0.11 / 0.20±0.26	0.09±0.04 / 0.21±0.16
East Siberian Sea	2.72 / 6.04	0.00 / 0.00	0.06 / 0.09	0.01 / 0.09

ACPD
15, 16775–16859, 2015

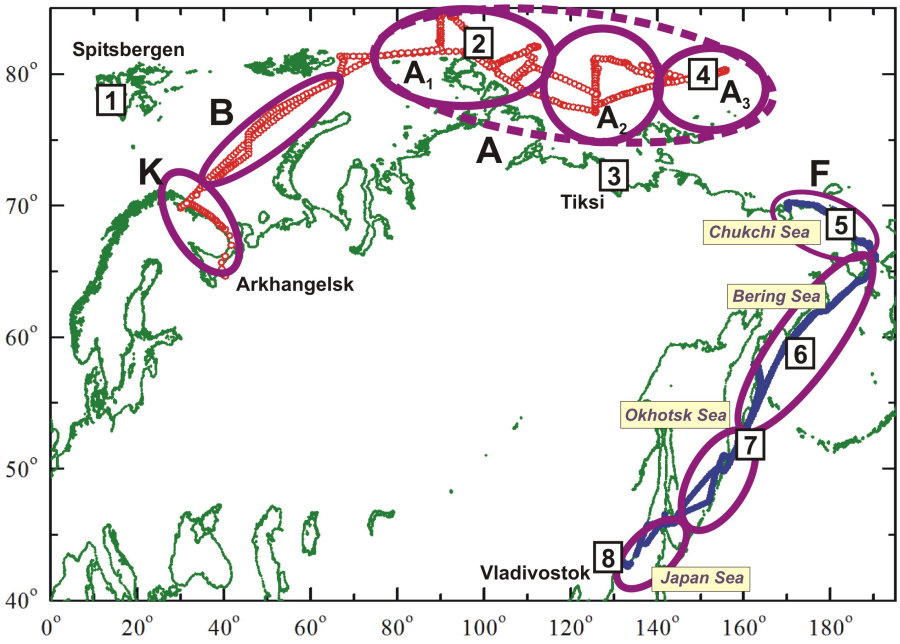

Figure 1. Map of the routes of Arctic cruises of RV *Akademik Fedorov* and *Professor Khljustin*: numbers indicate the regions where AOD values were calculated; letters and ovals indicate the sections of the routes within which the aerosol microphysical parameters were determined.

ACPD
15, 16775–16859, 2015

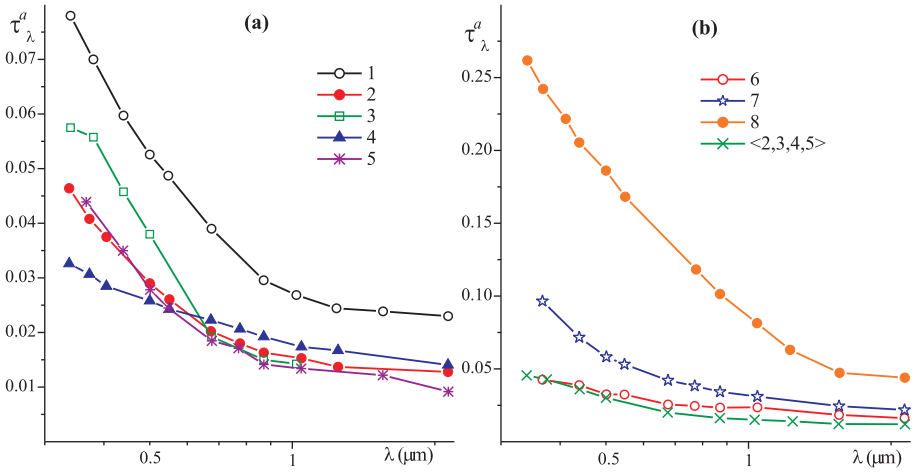

Figure 2. Average spectral dependences of AOD in the regions of **(a)** Arctic and **(b)** Far East seas (symbols $< 2,3,4,5 >$ indicate the average AOD values for the Arctic regions 2–5).

ACPD
15, 16775–16859, 2015

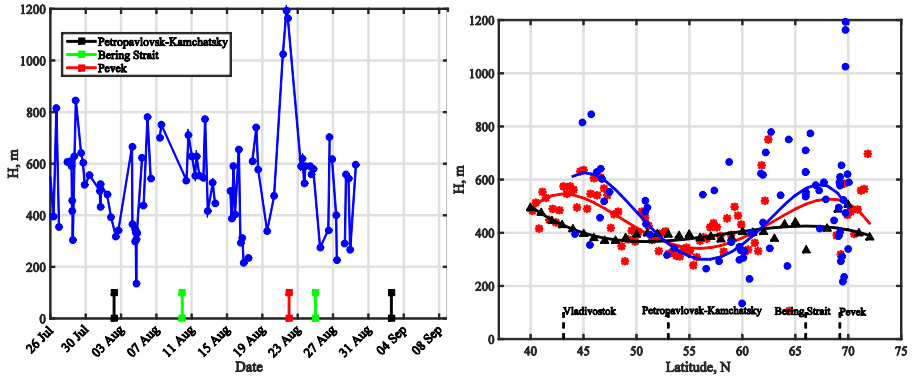

Figure 3. (a) The time behavior and **(b)** the latitudinal dependence of height H_{BL}, calculated according to data of ship-based measurements (blue circles), CALIPSO satellite (red asterisks), and ECMWF reanalysis (black line with rectangles). Solid lines show polynomial fits of the latitudinal dependence of H_{BL}.

ACPD
15, 16775–16859, 2015

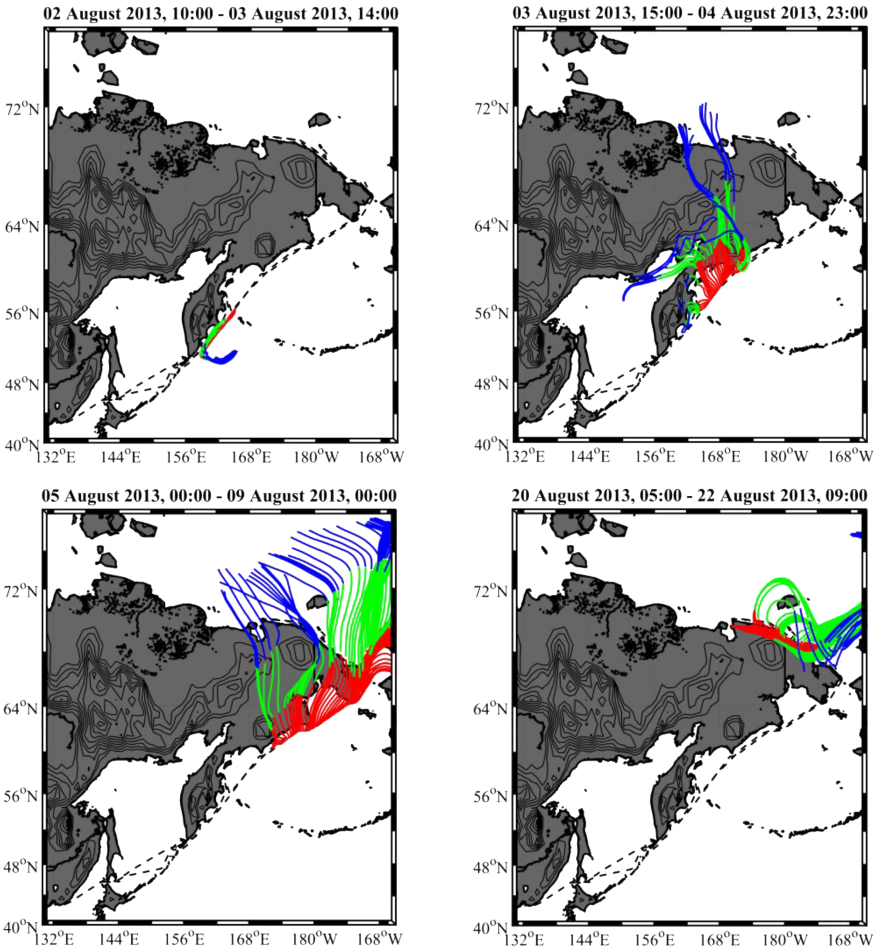

Figure 4. Trajectories of of air mass motion: red color is for the third day of motion of air masses, green color is for the second day, and blue color is for the first day.

ACPD
15, 16775–16859, 2015

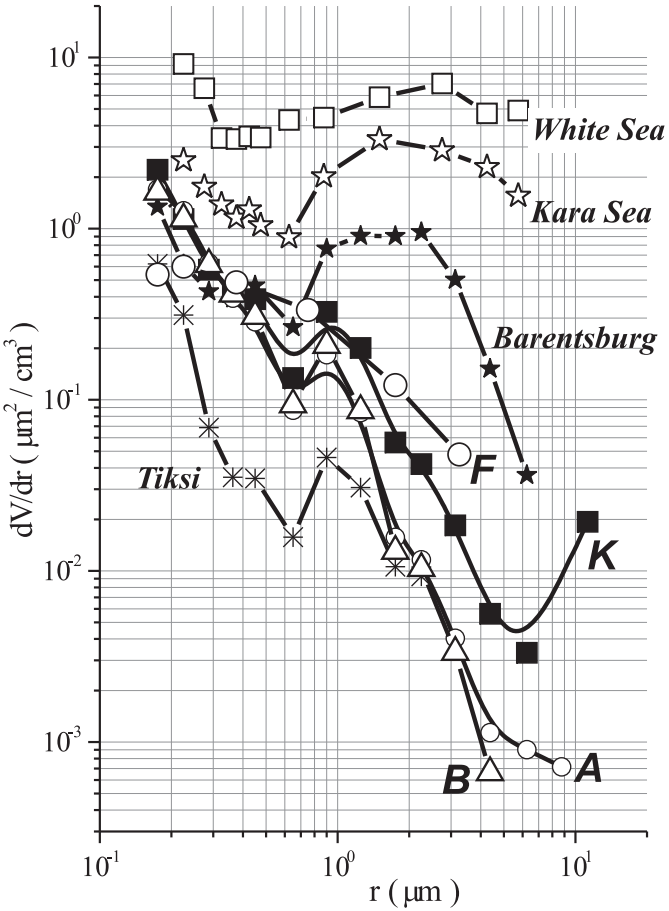

Figure 5. The average volume distributions of aerosol particles dV/dr in the regions K, B, A, and F as compared to analogous data in the White and Kara Seas, in Tiksi, and Barensburg (Sakerin et al., 2012).

ACPD
15, 16775–16859, 2015

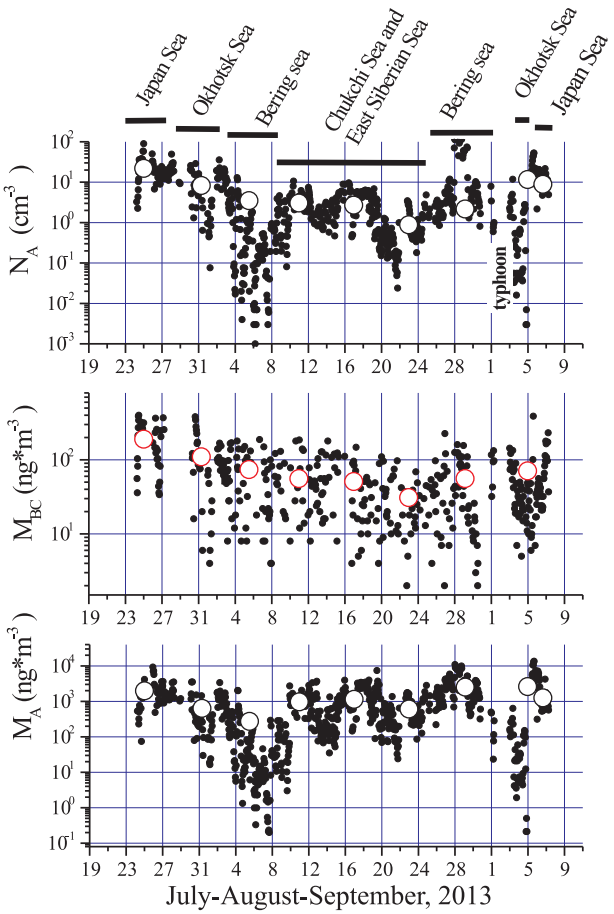

Figure 6. Time behaviors of the parameters N_A, M_A, and M_{BC} on the route of RV *Professor Khljustin* (circles indicate the average values of the parameters in water basins of separate seas).

ACPD
15, 16775–16859, 2015

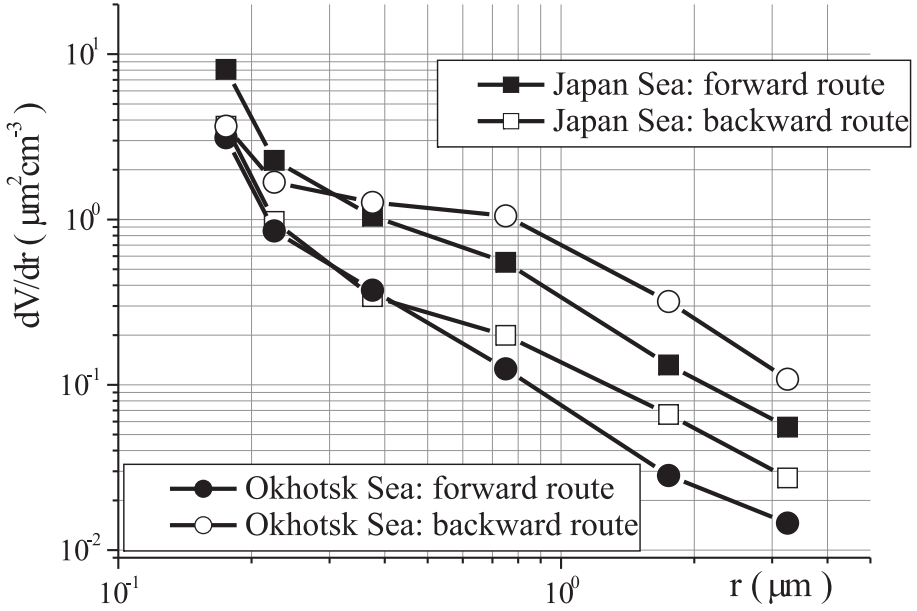

Figure 7. The average volume distributions of aerosol particles over the Japan and Okhotsk Seas, obtained on the forward and backward routes of RV *Professor Khljustin*.

ACPD
15, 16775–16859, 2015

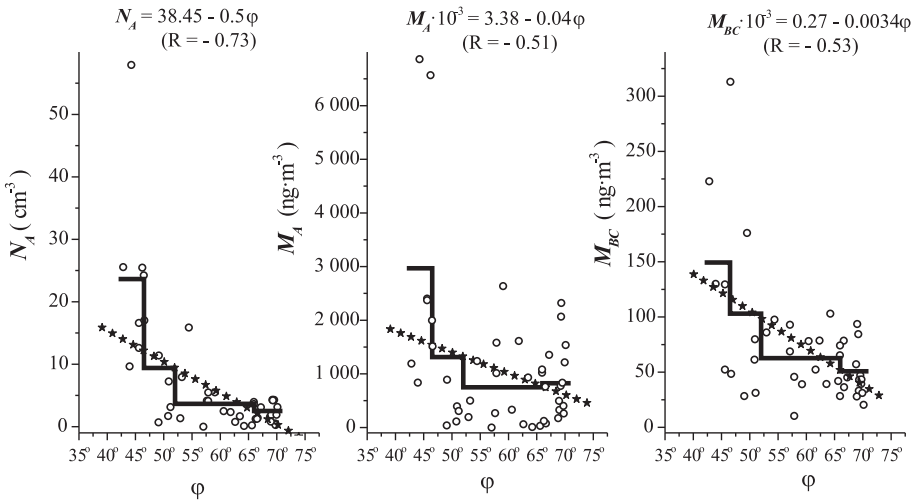

Figure 8. Latitudinal distribution of parameters N_A, M_A, and M_{BC} in Far East seas: asterisks indicate the linear regression, and thick lines indicate the average values within separate latitude zones.

ACPD
15, 16775–16859, 2015

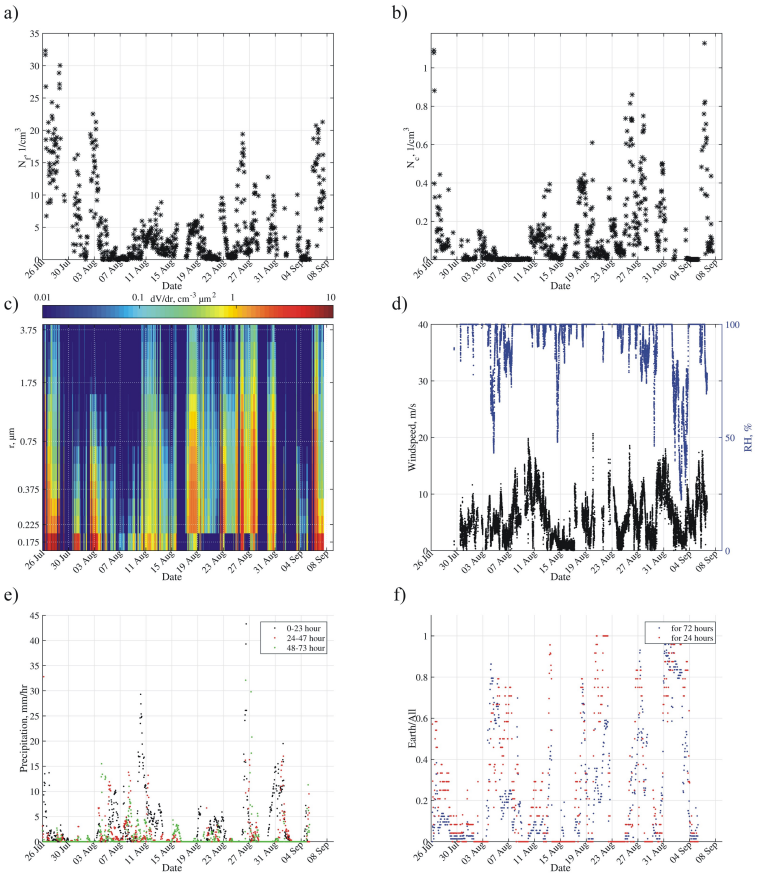

Figure 9. Time behaviors of the **(a)** number concentrations of submicron N_f and **(b)** coarsely dispersed N_c aerosol fractions; **(c)** the volume particle size distributions dV/dr; **(d)** the wind speed (black) and the relative air humidity (blue); **(e)** the along-trajectory rainfall amount; and **(f)** the fraction of trajectories passing over land.

ACPD
15, 16775–16859, 2015

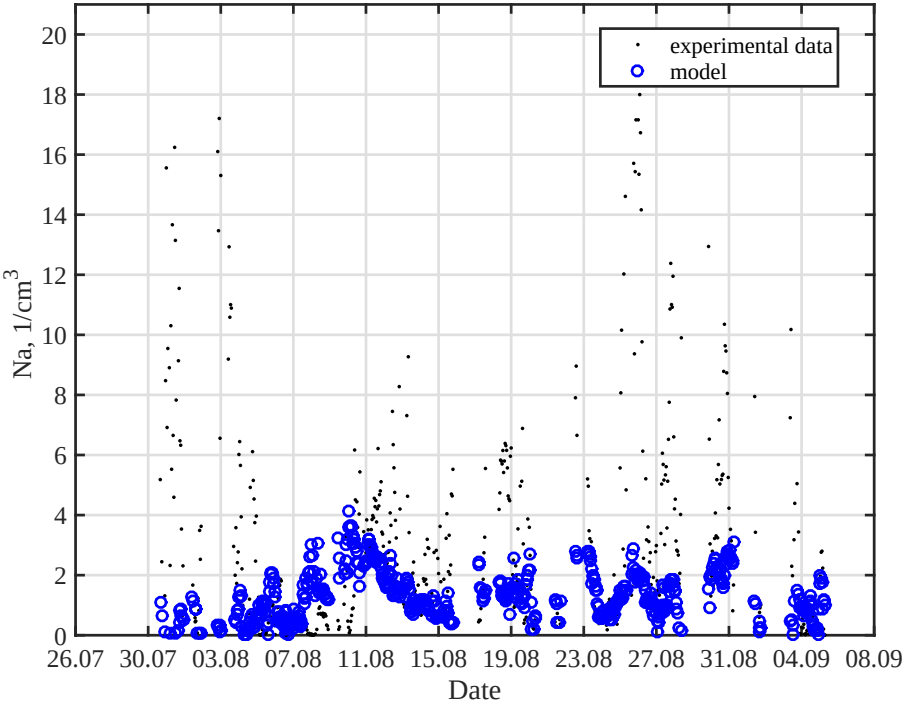

Figure 10. The measured and model (calculated) values of the aerosol number concentration.

ACPD
15, 16775–16859, 2015

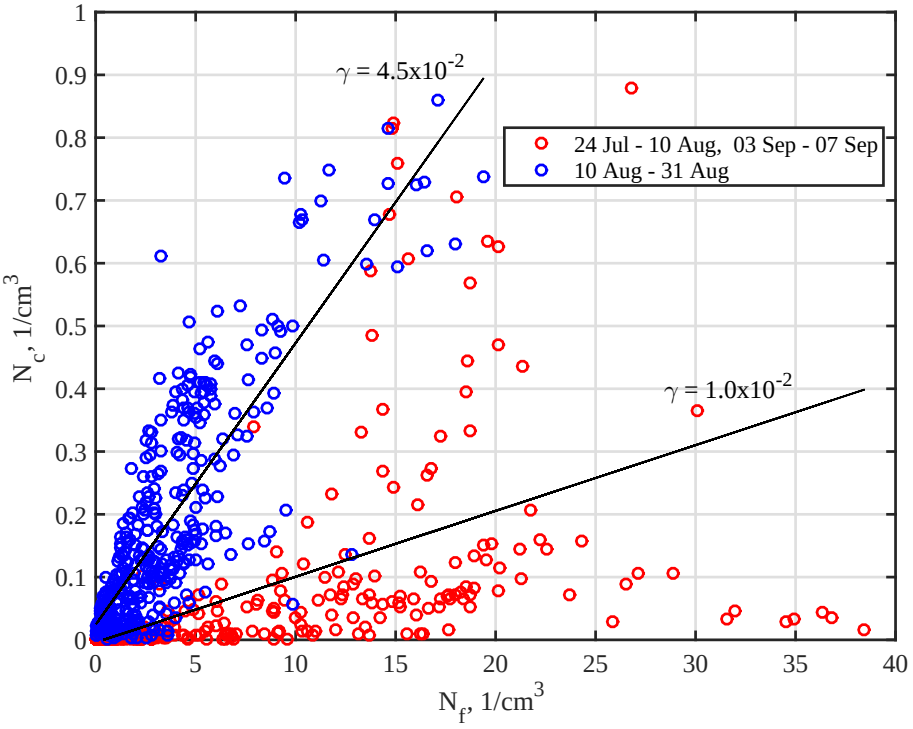

Figure 11. The scatter diagrams of number concentrations of submicron N_f and coarsely dispersed N_c aerosol at middle (red) and high (blue) latitudes.

ACPD
15, 16775–16859, 2015

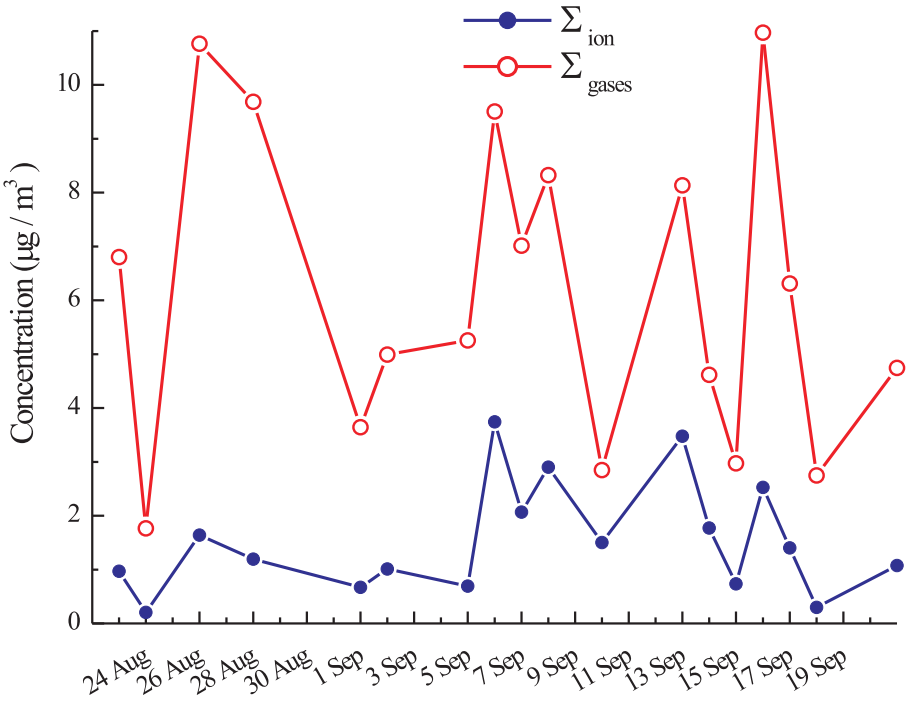

Figure 12. Interrelation between concentrations of the sum of ions in aerosol and gaseous impurities in the atmosphere along the route of RV *Akademik Fedorov* (August–September 2013).

ACPD
15, 16775–16859, 2015

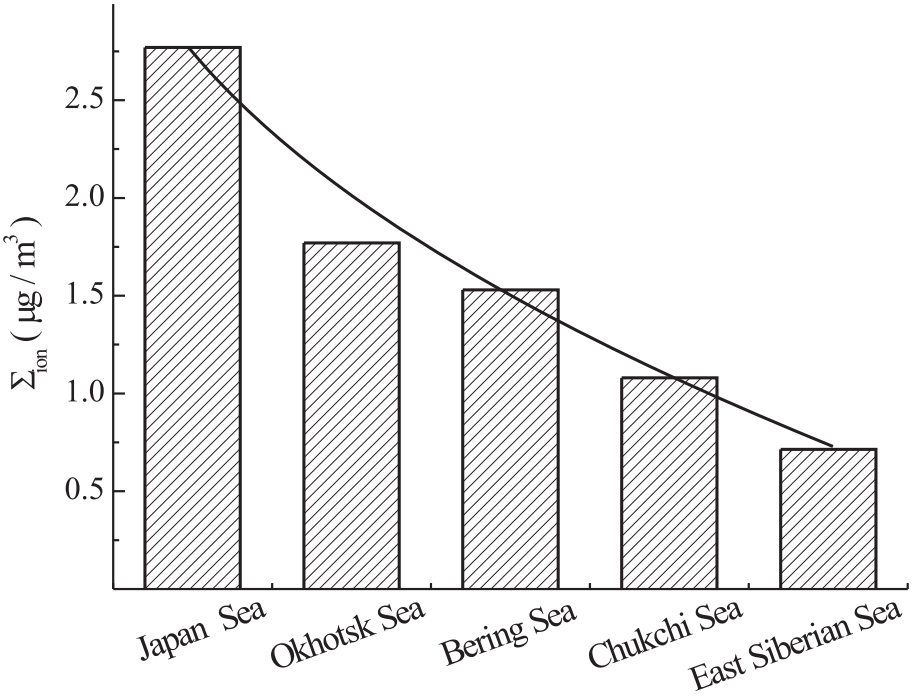

Figure 13. Latitudianl dependence of the mean sum of ions in aerosol in μg m^{-3} over water basins of Far East seas (July–August 2013).

ACPD
15, 16775–16859, 2015

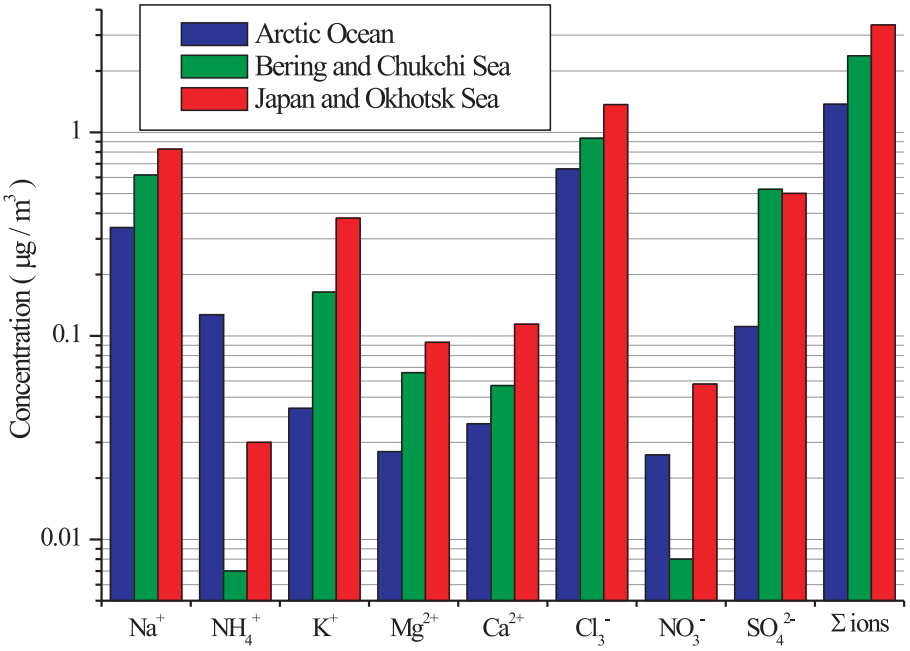

Figure 14. Average ion content in aerosol over Arctic and Far East seas.

ACPD
15, 16775–16859, 2015

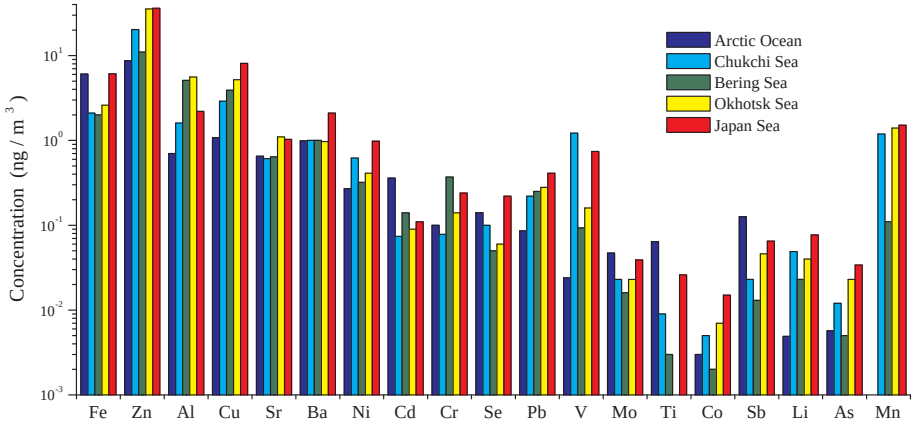

Figure 15. Average concentrations of elements in aerosol composition over Arctic and Far East seas.

ACPD
15, 16775–16859, 2015

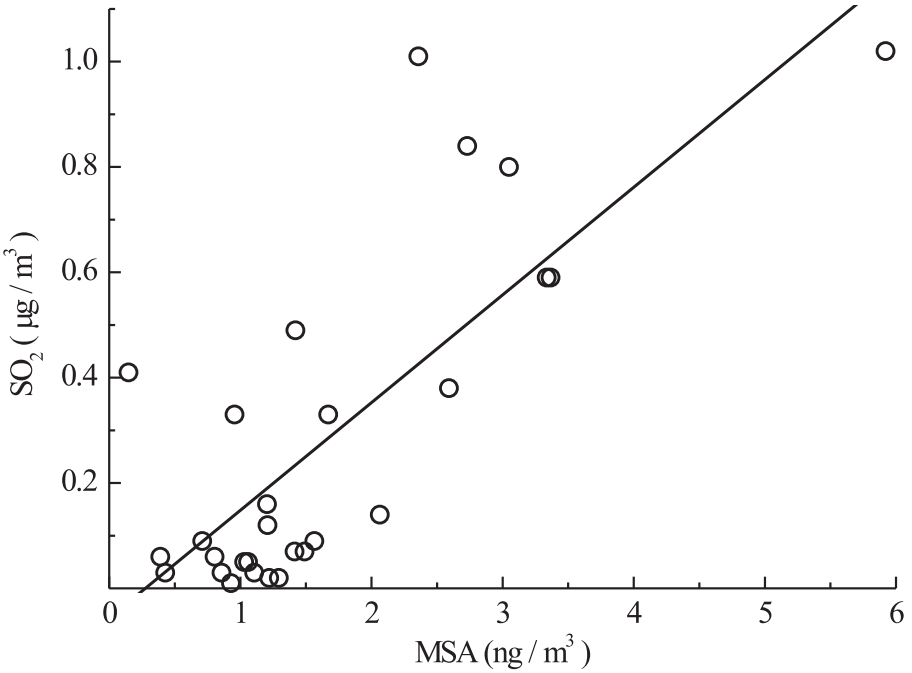

Figure 16. Interrelation between the MSA and SO_2 concentrations over Far East seas (July–August 2013).

ACPD
15, 16775–16859, 2015